MODELING AND SIMULATION OF *Trypanosoma Cruzi* USING COARSE-GRAINED METHODS

A new approach to Chagas disease research

by

Alberto Mario Castillo

Supervised by

Gabriel Villalobos Camargo

Professor, Dr. in Science - Physics

Thesis

Presented in partial fulfilment of the requirements for the degree of

Master of Science in Modeling and Simulation

Department of Basic Sciences and Modeling

Universidad de Bogotá Jorge Tadeo Lozano

Colombia

February 2022

ABSTRACT

This work presents the coupling of a model of the infective form of the *T. cruzi*, the causative agent of Chagas disease, with a model of blood flow. A network of harmonic springs was developed to represent the cell body, and the Dissipative Particles Dynamics (DPD) method was implemented to produce laminar flows. Parameters of the cell body structure were extensively searched to grant its stability and cell motility is the result of the transition between different cell shapes obtained after the motion of the parasite was discretized. Agreement of the blood flow to the characteristic velocity distribution was confirmed, as well as the fulfillment of the Fluctuation-Dissipation theorem.

Once the models were integrated, information on cell dynamics in response to different laminar flows was retrieved. It was found that results on cell elongation correspond to those from experiments. Partial agreement with *in vivo* assays was obtained for the center of mass displacement, and the energy consumption correlation with flow velocity derived in the proposal of a possible trade-off strategy for energy compensation.

In loving memory of

Luna and Calixto Castillo

This is a kite you never got to see up in the sky
but be sure, because of you into the deep blue, it can fly.
No one else but me can tell,
your writing style is everywhere.

Over your beloved tall grass field, it soars
the wagging of your tail, my happiness restores
Whenever I felt sad or overwhelmed
You were by my side, my forever friend.

ACKNOWLEDGMENTS

I would like to express my biggest gratitude to my esteemed supervisor, Dr. Gabriel Villalobos Camargo, for his always kind guidance, his unbeatable commitment, and all of his support during the entire research process. For teaching me about the core topics of this thesis and also on how to handle some of my issues, like what used to be my sometimes excessive perfectionism or my inability to ask for help when in need. Above all, I'm thankful for believing in me when others attempted to undermine my self-confidence.

I am grateful to the Max Planck tandem group from Universidad de los Andes because I got really useful insights from Dr. Helgi Ingólfsson and Dr. Gerhard Hummer during the conferences in the School of computer simulations of biological membranes and free energy calculations of biomolecular systems.

My gratitude is extended to Dr. Favio Cala Vitery and Jhoana Fonseca for their patience and the support they provided on the administrative tasks.

I would like to thank Ivy, who has been around since the very beginning of this adventure and in whom, through many interesting discussions and endless support, I could approach the biological concepts I needed to better understand this system from a biologist's point of view. Also, to Dr. Károly Jambrovics from Debrecen University for his outstanding gummy bear-based explanations on biochemistry topics.

My appreciation also goes out to my dear friends Jose Gómez, Daniel Grass, Alexander Hernández, Julio Alejandro Ortiz, Ricardo Londoño, Germán Eduardo Torres, Alejandra Cabarcas, Henry Jr. Garzón, and my taekwondo master Mauricio Puentes Forero who were always cheering me up.

I am very thankful to all of my family but especially to my inspiring mom, Mery Castillo, who said she has no idea about what I've been doing during the last years and to whom I want to confess: sometimes, neither I did. In the same line is my brother Adolfo Castillo, who on a monthly basis asked me if this work was finished and, of course, most of the time he did with a meme on never-ending theses, which turned out to be very helpful to improve my patience and understand how persistent he is.

And last but certainly not least, Miguel Ángel, thanks for being unconditionally supportive during the final track of this project, I'm aware this took away a lot of our time, but I do really admire the way you have handled the whole situation, and I am deeply grateful for how understanding you have been.

Contents

List of Figures

List of Tables

List of Abreviations

ATP Adenosine-triphosphate

DPD Dissipative Particle Dynamics

eATP extracellular Adenosine-triphosphate

MLE Maximum Likelihood Estimate

PCR Polymerase Chain Reaction

Pf-RBC *Plasmodium Falciparum* infected red blood cells

RBC Red Blood Cell

SAPA Shed Acute Phase Antigen

1 INTRODUCTION

Chagas disease or American Trypanosomiasis is caused by *Trypanosoma cruzi (T. cruzi)*, a protozoan parasite that flows within blood; while living and reproducing inside its human host for several years, the parasite would cause different diseases and even death[88]. The parasite is transmitted to humans mainly by blood-sucking insects but also through organ transplantation or congenital transmission[81]. During its life cycle inside the human body, *T. cruzi* causes cell lysis with subsequent tissue damage, two main stages of the disease have been identified: acute and chronic.

In the acute phase of the disease, only a minimal number of patients could exhibit a wide range of symptoms from fever to hepatomegaly including heart failures among others. After one or two months Chagas evolves to an indeterminate or latent form which is the first moment of the chronic stage and is called so because is still unknown how the infection evolves from it to cardiac or digestive forms. During latent form, symptoms disappear and difficulty detecting the infection rises. In the meanwhile, the *T. cruzi* continues causing severe damage to organs, mainly heart, esophagus, and colon[16].

Disease progression is illustrated in figure 1:

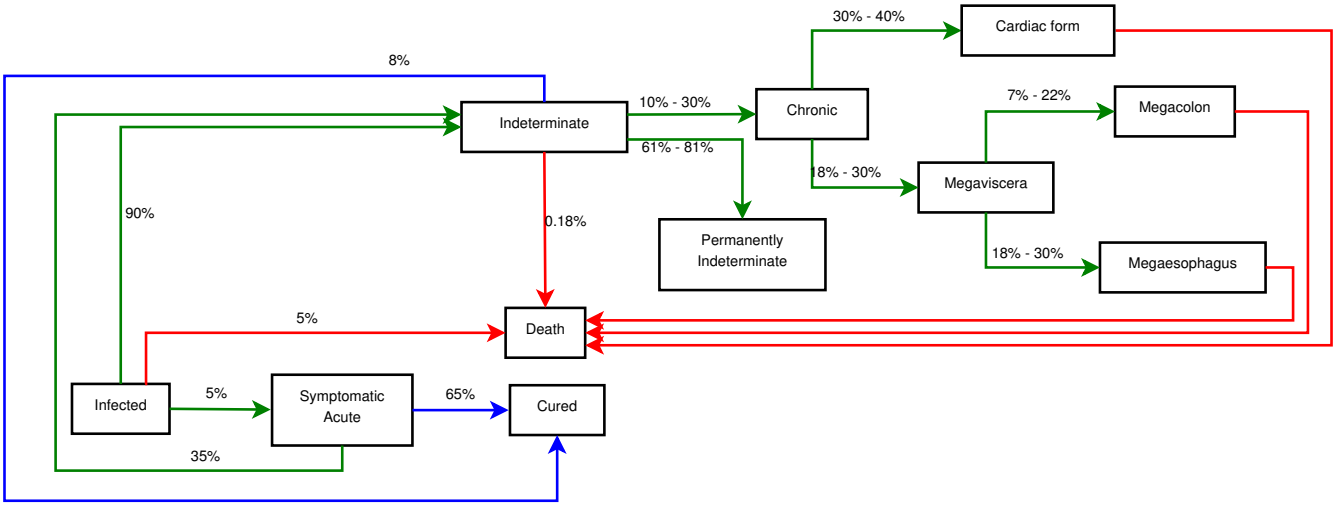

Figure 1: Patients transition between stages, cure, and death. Data from:[47],[70],[91], and [14]

Similarly to the process by which chronic stage is reached, the organ selection by the parasite is not completely clear. Melo and Brener [54] stated that variations among bloodstream forms of different parasite strains could lead to facilitate or prevent interaction with macrophages after finding several discrepancies in tissue infection. Following that line, parasite strains have been compared in terms of infection efectivity on specific tissue [3] resulting in possible explanations from a biochemical perspective. Despite this, the reason why the parasite arrives and manage to stay at those organs remains unclear; which is particularly striking if the differences in Reynolds number associated to bloodstream in each of them are taken into account:

Organ	**Artery**	**Reynolds number**	**Reference**
Colon	Superior and inferior mesenteric	702 - 1424	[48]
Heart	Right coronary	150	[92]
Esophagus (Thoracic)	Thyroid (Aorta communication)	600	[44]

Table 1: Reynolds numbers for different arteries

Due to migration, Chagas disease has spread around the world causing that almost eight million people worldwide are infected today. Is estimated that because of this neglected tropical disease every year 12500 people die, making it the parasitic disease in Latin America with the higher socioeconomic impact [64]. Such recognition not only

obeys to cardiovascular morbidity but to the premature death of patients that are economically productive, aged in the range of 20 to 50 years.

Incidence of Chagas disease is hard to measure because during acute stage only 1% to 2% of patients exhibit symptoms so most of infected population goes to indeterminate stage without diagnosis and remains there between 10 to 30 years[91]. Being incidence decisive to identify how much governments and health systems should invest on control and treatment programs, in 1990 Hayes and Schofield[33] using pathology prevalence and Latin America birth rate, estimated 850000 new infection cases per year.

Initiatives in endemic countries have been focused in vector control and providing access to drug treatment, impacting on incidence and prevalence respectively. Significant progress was achieved in two decades[91]:

Year	Deaths per year	People infected	Prevalence
1980	45000	16 - 18 Millions	4.72%
2005	23000	10 - 14 Millions	3%

Table 2: Pathology epidemiological evolution

Particularly for Colombia in 2004 was estimated that 1300000 people served as *T. cruzi* host with 78% of patients demanding an average of $US\$1028$ for treatment per year including basic, intermediate and specialized services while the other 22% never accessed to the health system due to this pathology [14].

Chagas disease is curable when the infection has just started but there is a lack in access to diagnosis and due to this, to treatment. Existing methods to detect the pathology are facing issues regarding sensitivity, that in best cases -Polymerase Chain Reaction (PCR) assays- ranged from 44.7% to 90%[7] and in order to avoid false positive or negative results, several additional tests, as blood screening, have to be used. This deficiency becomes critical during chronic stage when the parasitaemia level becomes almost unnoticeable while focal lesions appear on patients tissue. The cause of these lesions is still a matter of discussion but what is clear so far is the need to increase the understanding of the parasite and its interactions with the host [68]. To this end, many research initiatives have been launched under different approaches, for example: cell biology, biochemistry, drugs design, vaccines development, new laboratory techniques for diagnosis, disease transmission, and vector control among others.

Unfortunately, those efforts have not been able to provide enough insight into the evolution of the disease and parasite tropism, both of which are phenomena that modeling and simulation has the potential to help better understand. This new approach will start by supporting exploration of *T. cruzi* physical structure and mechanical properties through spring network models and coarse-grained methods, becoming the basis for further research in the field delving into other topics such as interaction with blood corpuscles or human tissues.

1.1 Red Blood Cells

Erythrocytes or Red Blood Cell (RBC) are specialized cells in charge of gas exchange between lungs and tissues in vertebrates. The term specialized does not only refer to the function that they execute but to its structure which in order to maximize their surface area to volume ratio presents absence of organelles, such as mitochondria or nucleus in mature cells of mammals[4]. This remarkable function could not be carried out without specific mechanical and rheological properties as bending resistance or membrane viscoelastic behaviour, that are still under research and allows this biconcave shaped cells with a diameter close to $7.8\mu m$ pass through capillaries with about $4\mu m$ in diameter. While erythrocytes flow in blood not only exhibit extreme deformation, also a response to flow rate is shown due to the interaction among them producing aggregation or dissociation[93].

1.1.1 Erytropoiesis

Depending on mammalian age and stimulated by erythropoietin, red blood cells can be produced in yolk sac, liver, spleen, and bone marrow[10]. Before reaching mature, nucleus and other structures are expelled from the cell and then, the cell is released to bloodstream where after one or two days will turn into an erythrocite with a life span close to 120 days[9].

1.1.2 Function

Red blood cells' lack of nucleus seems to be the evolution response to increase their transport capacity, day by day this cells are permanently supporting gas exchange process: carrying oxygen from lungs to tissues and retrieving carbon dioxide from tissues to the lungs[4].

1.2 *Trypanosoma cruzi*

As mentioned before, *T. cruzi* is a protozoan, an unicellular organism with organelles and genetic material contained in its nucleus. *T. cruzi* lives inside tissues of both vertebrates and invertebrates, by using different forms it can replicate by binary fission and transport within blood flow to spread itself in host body[78].

1.2.1 Nymphal stages

Capability of *T. cruzi* to adapt to different hosts is remarkable, six differente stages have been identified so far[34]:

1. *Amastigote*
2. *Choanomastigote*
3. *Promastigote*
4. *Opisthomastigote*
5. *Epimastigote*
6. *Trypomastigote*

The flagellum is not present in the *Amastigote* stage and for the others it emerges at different positions from some sort of pocket. In the *Choanomastigote*, *Promastigote*, and *Opisthomastigote* is located at the anterior tip while in the *Epimastigote* and *Trypomastigote* it comes along the side.

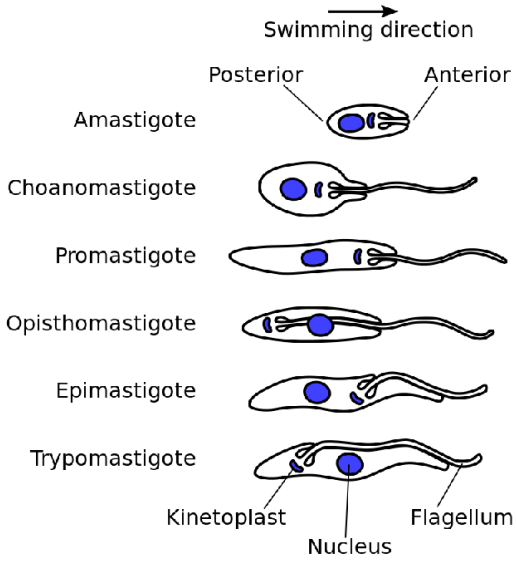

Figure 2: *Trypanosoma cruzi* nymphal stages[89]

Inside mammals Not all nymphal stages are present when *T. cruzi* parasites in mammals; the infection starts when *Trypomastigotes* are deposited on host by infected *Triatomines* and the parasite trespass mucosal surface. Once they reach host cells will differentiate into *Amastigotes* to replicate and will change again into *Trypomastigotes* to spread the infection while flowing with blood.

1.2.2 Transmission

The parasite is mainly transmitted to mammalians by *Triatomines*, a family of blood-sucking insects where *T. cruzi* has been identified in its *Trypomastigotes* and *Epymastigotes* forms; being the first used to entry and exit from the insect body and the second, the reproductive form[70]. At this point it is important to mention that parasite reservoirs can be found in several orders of mammalians as Chiroptera, Canidae, Didelphimorphia, and Primates among others, revealing a complex transmission system[39]. Even in nonendemic areas with infected *Triatomine* population under control, if contact between such reservoirs secretion and food exist the disease will appear[76].

1.2.3 Infective form structure

Bloodstream trypomastigote is the infective stage, present in blood, it has single nucleus and continuous flagellum along the membrane[21]. Parasite plasma membrane is not homogeneus, density and intramembranous particles produce a division into three macrodomains[80]: cell body, flagellum and flagellar pocket.

Besides being the smallest macrodomain,flagellar pocket plays a major role defining cell motion because its position is associated with speed improvement[2].

Following [80], a brief description of intraparticles inside cell structure and organelles is listed below:

1. Cytoskeleton: A set of subpellicular cross-linked microtubules distributed along the cell body[31].
2. Kinetoplast: Network of crosslinked circular DNAs[74].
3. Glycosome: Spherical structures within a homogeneus matrix[80].
4. Acidocalsisome: Rounded vacuoles bounded by a membrane used to store acidic calcium[22].
5. Contractile vacuole: Tubules network connected to a central vacuole[80].
6. Lipid inclusions: Granules without membrane around[56].
7. Secretory pathway: Set of tubular and vacuole-like structures from one side to another inside the parasite[52].
8. Endocityc pathway: A network of vesicles and tubules from anterior to posterior parasite body that at its end fuses with reservosome[20].
9. Reservosomes: Spheres surrounded by membranes, it disappears when the parasite differentiate to trypomastigote infective form[17].
10. Nucleus: Single sphere of almost 2μm length that has a membrane with pores around it[79].

A comparison among trypomastigote and host cells is presented in [Tab. 3]:

Cell	Length	Width
	12 to 26μm [82]	1 to 2μm [61]
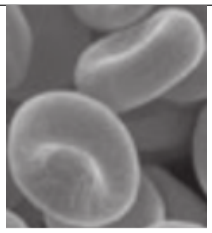	7.4 to 8.2μm [9]	0.8 to 2.6μm [4]
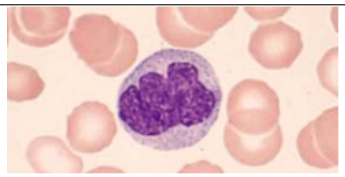	12 to 18μm [23]	
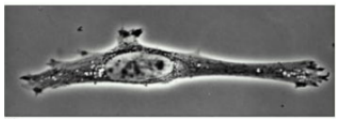	30 to 50μm [1]	

Table 3: Images from top to bottom are: Blood trypomastigote[82], red blood cells[11], monocyte (phagocityc cell)[71] and fibroblast (non-phagocytic cell)[73]

1.3 Chagas Symptomatology

At each stage of the disease the symptomatology varies substantially making the infection harder to detect by conventional methods.

1.3.1 Acute stage

Corresponds to first six to eight weeks of infection, it is identified in almost 1% of infected patients and causes among others: chagomas which is a skin reaction in the place used by the parasite to access host body, also myocarditis, convulsions, Romaña's sign or meningoencephalitis [62], occurring the latter mostly in children within the first two years of life[69].

1.3.2 Chronic stage

One or two months after infection begins it becomes undetectable, a fall of parasitaemia level and the associated symptoms disappearance are the fundamental reasons for this to happen. At this point of the disease, which is also called '*indeterminate form*', misdiagnosis and complications associated with late treatment are susceptible to take place [16]. Individuals that reach this phase can survive decades infected. Nevertheless, tissue damage never stops, is not reversible and leads a minority population to present severe consequences at heart, digestive or nervous system[58]. According to [50] the pathology form at chronic stage is related with genetic factors,it means, some hosts are genetically prone to develop the cardiac form rather than the digestive and vice versa. It is important to mention that patients at chronic stage can exhibit symptoms from acute stage if their immune system is suppressed,

unfortunately this interruption, may be as an option to provide treatment for concurrent infections, can also derive in misdiagnosis or delay in Chagas' disease treatment[67].

1.4 Rheology

Presence of parasites by itself can cause plasma viscosity growth, however the entire variation in bloodstream during Chagasic infection can not be fully awarded to them. Additional reasons found in [8] are:

1. Enhancement of γ-globulin levels as a result of host response to infection.
2. *Trypanosoma cruzi* Shed Acute Phase Antigen (SAPA) produces neuraminidase, an enzyme that cause declination of red blood cells membrane fluidity.
3. Throughout the inflammatory process, nitric oxide levels are raised reducing erithrocyte deformability with subsequent limitation to flow trhough capillaries.

1.5 Cell invasion

Trypanosoma cruzi interaction with host cells aiming to invasion can be divided in three major processes with specific variations depending on the type of host cell, *T. cruzi* strain and developmental stage[19].

First process is *adhesion and recognition*, it takes place at membrane domain and is produced by molecular recognition at host cell receptors. The parasite use a wide set of molecules to interact with macrophages and non-macrophages cells, former ones can be deactivated by trypomastigotes phosphatidylserine present in its surface.

Main cell *internalization* mechanism in macrophages is phagocytosis but the parasite can get into cells through endocytosis or membrane invagination once host cell receives appropriate signaling from intruder.After invasion, a structure named parasitophourus vacuole is produced inside the cell allowing trypomastigotes turn into amastigotes,during this transformation, vacuole membrane is lysed exposing amastigotes to cytoplasm and triggering binary fission. When the entire host cell rupture occurs, amastigotes are liberated into bloodstream where they can continue spreading the infection by itself or turning into trypomastigotes.[40]

1.6 Modeling of the motility, rheology, and mechanical response of flagellated swimmers

1.6.1 Coarse-graining

The use of multiscale modeling in soft matter allows to simulate nanometer scales as well as large scale dynamics. It has been used to predict the flow resistance enhancements at different parasitaemia levels in *Plasmodium Falciparum* infected red blood cells (Pf-RBC) [25], study the effect of temperature in the mechanical and rheological properties of infected blood in malaria [28], investigate the adhesive dynamics of Pf-RBC as function of wall shear stress and other parameters[27], and study the flow-induced clustering and alignment of vesicles and red blood cells in microcapillaries [53].

Typical length and timescales that are usually addressed by these models are given in [Tab. 4].

Characteristic	**Value**	**Reference**
Mean curvature R_0	3.4 μm	[53]
Capillary Radius R_{cap}	1.4 R_0	[53]
Vessicle length L_{ves}	1.5 - 3.88 R_{cap}	[53]
Number of vesicles n_{ves}	6	[53]

Table 4: Parameters from a red blood cells model

1.6.2 Flagellated Swimmers

At low Reynolds numbers inertia does not play an important role in the locomotion of single cell organisms [46]. Current research aims to both: understand biological systems as well as to create synthetic versions that may be

used for medical applications. For instance, Williams et. al. were able to design and build a synthetic swimmer, (2 mm long and 20 μm thick) giving proof of concept of a design of a biological machine [90].

1.6.3 Spring Network Models

Predominantly based on Hooke's law and consctructed including beads as nodes connected by normal, shear or rotational springs [24], these models can represent several systems in 2D and 3D domains in order to explore mechanical properties or crack propagation phenomena [18].

Omori et al.[63] found that for biological membranes, spring networks cannot easily represent area incompresibility and have a high mechanical properties dependence on the mesh configuration. Those limitations could be partially explained by the need of empirical definitions [32] of unexplored systems parameters and functions, which is also a concern regarding physical agreement of the results. Notwithstanding, recently simulations of trypanosomatid parasites[2] and flagellated bacteria[42]have been successfully implemented to explore motility pattern and replicate cell body structure.

A spring network representation is shown below3:

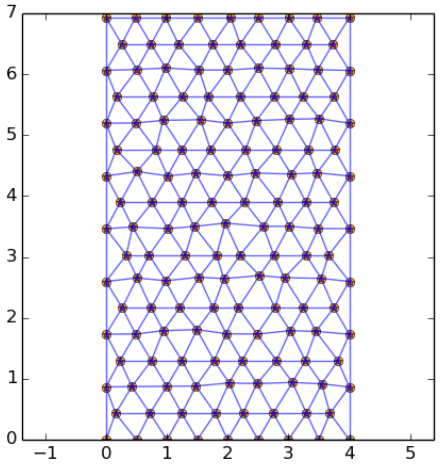

Figure 3: Spring network used to study bamboo cracking propagation in [87].

2 AIM OF THE STUDY

As a contribution to bridging the gap on understanding the evolution of parasite-host dynamics during Chagas disease, this thesis aims to identify the effect of different laminar blood flows over bloodstream trypomastigote mechanical properties. In this way, modeling and simulation will help to clarify if the parasite tropism is not only a matter of genetics or biochemical interactions at the membrane level but driven by the dynamics between blood flow and the cell body. To enable this new research approach on Chagas disease we propose:

1. To model the parasite cell body via a spring network to simulate its motion.
2. To model the blood flow at different Reynolds numbers by means of a coarse grained method to simulate the flow-parasite interaction.
3. To identify, through the analysis of the simulations results, if the parasite mechanical properties response to different flows could explain its tropism in the human body.

3 MODELS AND METHODS

The present project aims to use computational physics models to provide some insight into the mechanical interaction between the bloodstream trypomastigote and the blood flow.

The trypanosome body is modelled using a spring network structure to represent the cell membrane. The structure of the body is defined by a two dimensional triangulated network of N_t triangles, which in turn have a set of nodal points located at their vertices, N_n. The nodes are connected by N_s springs.

Let us call the set of coordinates of the nodes as: $\{\vec{x_i}\}$. The potential energy of the system is given by:

$$V(\{\vec{x_i}\}) = V_{elastic-membrane}(\{\vec{x_i}\}) + V_{area}(\{\vec{x_i}\}) \tag{1}$$

With this model definition we depart from [26], who in turn uses a 3D model of a red blood cell including many more interaction terms.

In the case of blood flow, it is modelled by means of a mesoscopic method in which fluid particles are aggregated, such aggregations interact in defined phases [36]. Model agreement to hydrodynamic behaviour is confirmed by assessing the velocity distribution and the fulfilment of the Fluctuation-Dissipation theorem. Finally, we implemented the Poiseuille flow adaptation of the model [5] to obtain the ability to adjust the flow and reach the Reynolds numbers corresponding to the parasitized organs.

To summarize, we will be using two main computational methods: Dissipative Particle Dynamics and Spring Network.

3.1 Dissipative Particle Dynamics (DPD)

Dissipative Particle Dynamics (DPD) models are useful at the mesoscale level, when hydrodynamics and thermal fluctuations are at play. A DPD particle represents a group of the molecules of the fluid under study, thought of as a coarse grained blob. They move off-lattice and interact via three kind of forces: a conservative one(2), arising from a potential; a dissipative force(3), that smooths out the radial differences between particles; and a stochastic force(4), in the direction between particles[60].

Let's use [60] to explain the forces

$$\vec{F}_{ij}^{C} = F_{ij}^{(c)}(r_{ij})\vec{e}_{ij} \tag{2}$$

$$\vec{F}_{ij}^{D} = -\gamma\omega^{D}(r_{ij})(\vec{v}_{ij}\cdot\vec{e}_{ij})\vec{e}_{ij} \tag{3}$$

$$\vec{F}_{ij}^{R} = \sigma\omega^{R}(r_{ij})\zeta_{ij}\vec{e}_{ij} \tag{4}$$

Here, $\vec{e}_{ij}$ is a unit vector pointing in the direction of the interaction, γ and σ are the strength of the dissipative and random forces respectively, ζ_{ij} is a Gaussian random variable with unit variance, and v_{ij} is the difference between particles velocities. The random and dissipative forces must satisfy the Fluctuation-Dissipation theorem, in that sense, those forces are not independent from one another, they are linked by:

$$\omega^{D} = [\omega^{R}(r_{ij})]^2 \tag{5}$$

$$\sigma^2 = 2\gamma k_B T \tag{6}$$

ω^R and ω^D are weight functions in (4) and (3). By definition, all forces are refrained to act beyond cut off distance r_c.The conservative force (2) follows this restriction through:

$$\vec{F}_{ij}^{C} = \begin{cases} a_{ij}(1 - r_{ij}/r_c), & \text{if } r_{ij} \leq r_c \\ 0, & \text{otherwise} \end{cases} \tag{7}$$

where a_{ij} is a coefficient representing the strength of the conservative force between particles i and j.

For the other forces, satisfying the cut off condition is a consequence of the weight function:

$$\omega^R(r_{ij}) = \begin{cases} (1 - r_{ij}/r_c)^k, & \text{if } r_{ij} \leq r_c \\ 0, & \text{otherwise} \end{cases} \tag{8}$$

Having $k = 1$ for the original DPD implementation.

The effect of the forces takes place under time evolution which, in fact, follows two main stages: collision (9) and propagation(10). The corresponding system of equations, as proposed in [36], is:

$$\mathbf{p}_i' = \mathbf{p}_i + \sum_j \Omega_{ij} \vec{e}_{ij} \tag{9}$$

$$r_i' = r_i + \frac{\delta t}{m_i} \mathbf{p}_i' \tag{10}$$

In (9) Ω_{ij} is the momentum transferred from particle i to particle j after an interaction occurs.

$$\Omega_{ij} = (\vec{F}_{ij}^C dt + \vec{F}_{ij}^D dt + \vec{F}_{ij}^R \sqrt{dt}) \vec{e}_{ij} \tag{11}$$

Here e_{ij} defined as the vector pointing from particle i to particle j.

We assessed the implementation via:

1. **Velocity distribution**: A set of 900 DPD particles interacted during 10000 internal time units. The velocity was measured and the following empirical distribution was obtained:

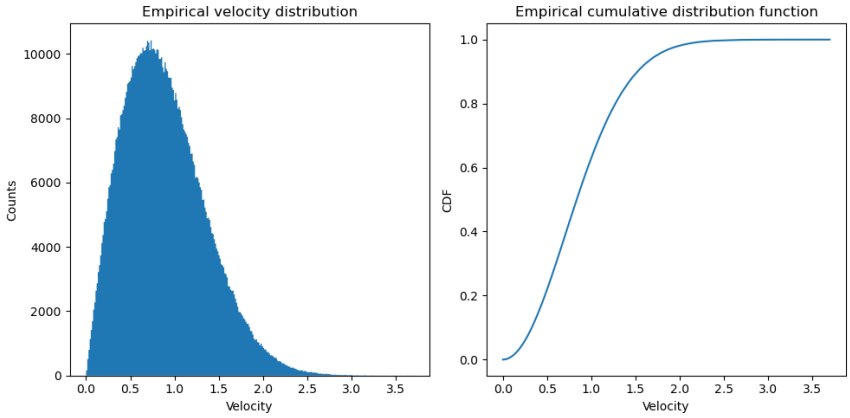

Figure 4: Empirical velocity distribution

The data was fitted to a Maxwell-Boltzmann distribution which contains only one parameter, the scale parameter, and its estimation was done by means of Maximum Likelihood Estimate (MLE) method complemented with a bootstrapping approach in an attempt to find a parameter as close to the population parameter as possible. The estimated scale parameter lies within the range of 0.5775 and 0.5802 as can be seen in 5:

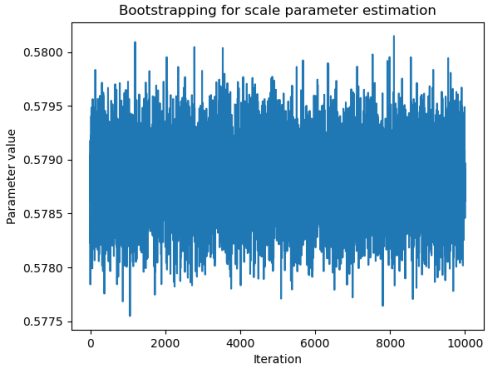

Figure 5: MLE results for the scale parameter

The probability density functions obtained by the MLE and its complementary bootstrapping were compared to the data histogram to visualize how close they are:

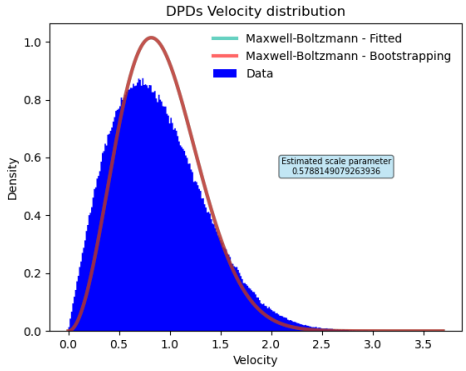

Figure 6: Particles speed distribution

To quantify the agreement of the estimated Maxwell-Boltzmann distribution to the data the probability plot is presented in 7a, in addition the cumulative density functions are compared in 7b. Differences between data and the estimated distribution could be explained by the behaviour on tails:

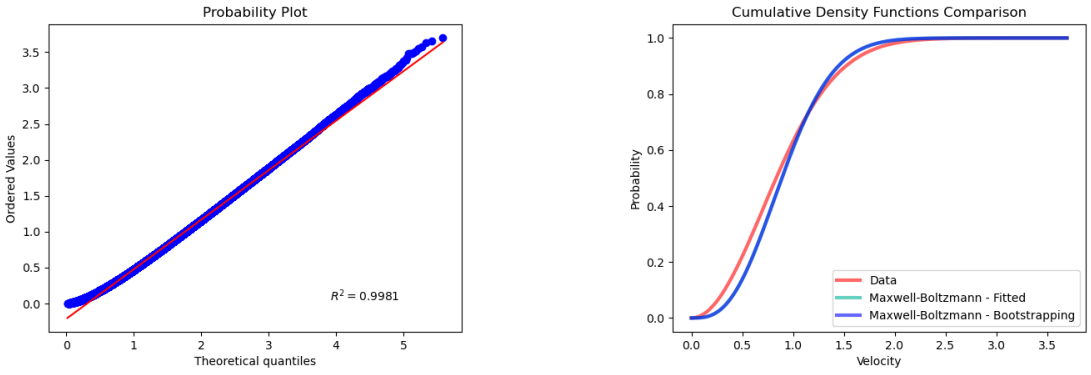

(a) Probability plot

(b) Cumulative density functions compared

Figure 7: Assessing goodness of fit

This is how it is possible to conclude that as well as in [36] the particles velocity follows a Maxwell-Boltzmann distribution.

2. **Thermostat**: Its function is to keep the temperature of the system constant. In agreement with the Fluctuation-Dissipation theorem, if the system dissipates energy there should be, as well, a reverse process increasing the fluctuation. In (3), γ is the parameter responsible for the viscous effect, it means, cooling down the system while the stochastic term ζ_{ij} in (4) is responsible for heating the system up. This relation implies that if the system temperature and in consequence its velocity tend to get too high -or too low, the correspondent force in (11) will dominate and drive the system towards an equilibrium state.

   To evaluate the behaviour of the thermostat the following experiments were performed:

   (a) Simulation of the system with increasing values of γ for a given value of σ

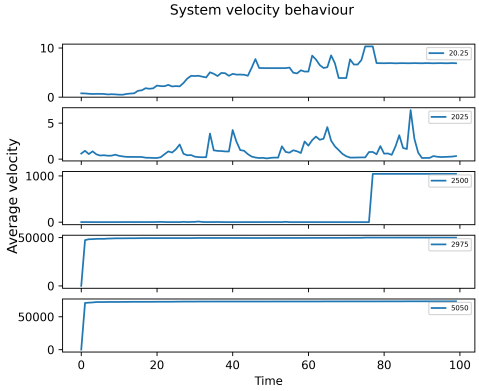

Figure 8: System velocity under the thermostat as a function of time for increasing γ values

   (b) Simulation of the system with increasing values of σ at a fixed value of γ

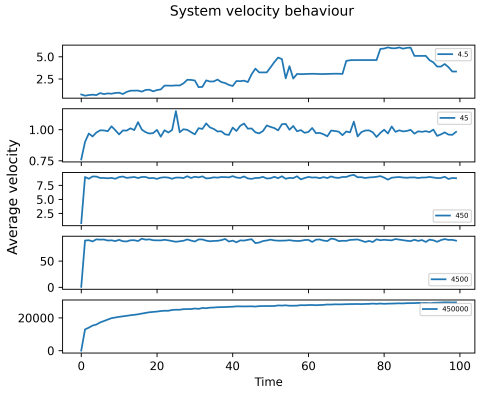

Figure 9: System velocity under the thermostat as a function of time for increasing σ values

As noted in the legends, the values we used to test for γ effect were $20.25, 2025, 2500, 2975$, and 5050, for σ the values were $4.5, 45, 450, 4500$, and 450000. In both sets of experiments, the system reaches a point close to equilibrium however the way it does, slightly differ between experiments. In 8 the damping term clearly domains the system leading the average velocity close to zero but once a threshold value of γ is surpassed the system velocity stabilizes under the domain of the random variable σ. On the other hand in 9, for the chosen set of values, the stochastic term rapidly takes control of the system causing the average velocity to increase. Such increase in system velocity has a limit, and again in each experiment, the system stabilizes around it as a result of γ viscous effect.

In this work, blood vessels are assumed as a rigid channel with periodic boundary condition applied on two sides selected in accordance to the direction of flow to simulate. Particles interaction occurs within the channel domain. It is well known that red blood cells represent almost 99.9% of blood cells [4] and immnune processes have an impact

on their performance, but since they are not parasitized by *T. cruzi*, they were not considered under the scope of this research, meaning our blood flow representation is closer to blood plasma.

It is important to keep in mind three limitations of DPD models. First, the linear conservative forces of DPD produces an unrealistic equation of state that is quadratic in density[1]. Secondly the DPD friction forces are too simplistic, due to the tangential nature. Thirdly, some macroscopic characteristics, as the friction, depend on the number density; changing the latter would imply reparametrization. "In other words, in DPD there is no notion of *resolution,grid refinement*, and *convergence* as in CFD" [2].

In DPD, as well as in other computational simulations of fluids, the viscosity must be measured. To this end, the so called Poiseuille method [5] provides a solution: to apply a body force to each particle in a different direction depending on the subdomain of the system where it is found. In our system, a constant force is applied on each particle in one axis direction and perpendicular to the remaining axis, the selection of the main axis depends on the flow to simulate -parallel or perpendicular:

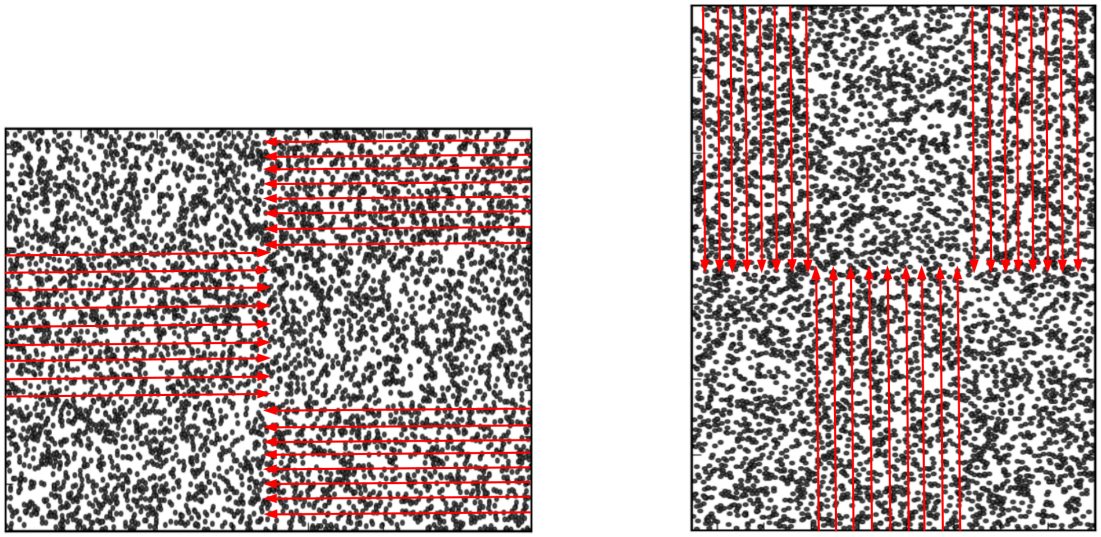

(a) Parallel flow

(b) Perpendicular flow

Figure 10: Channel configurations under Poiseuille approach

Hence the tensor has the form:

$$\tau_{yx} = \rho g_x (y - \frac{1}{2}D) \tag{12}$$

Where ρ is the fluid density, g_x is the force applied, and D is the length of the box. The velocity is calculated as:

$$V_x = \frac{\rho g_x}{2\eta}(yD - y^2) \tag{13}$$

In (13) η is the dynamic viscosity.

Proper implementation of the Poiseuille flow method is confirmed via the density profile 11, which should remain close to constant, and the velocity profile:

[1] R. D. Groot and P. B. Warren, J. Chem. Phys. 107, 4423 (1997)
[2] P. Español, P.B. Warren, J.Chem. Phys. 146, 150901, 2017

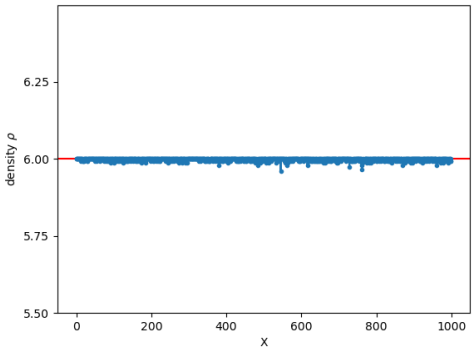

Figure 11: Density as a function of time: Measured profile (blue) and theoretical value (red).

Since the particles are exposed to a body force the expected velocity profile should be parabolic [5]. Such behaviour is consistent with the fully developed flow assumption for laminar flows [45], it is, at the beginning of the flow development a flat profile is present and should evolve into a parabolic one:

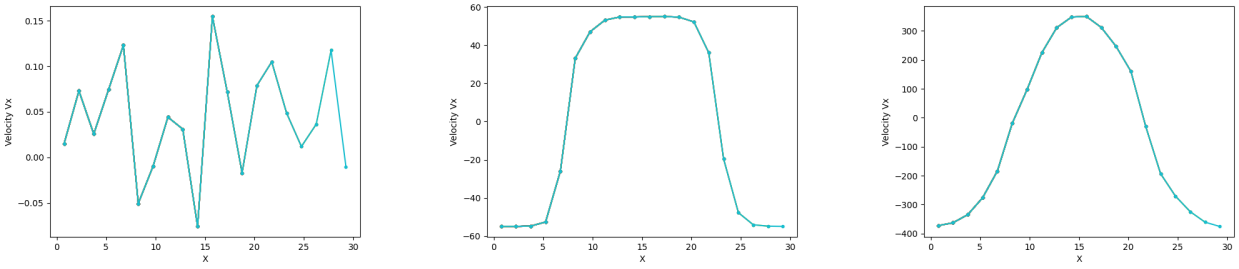

(a) Before appliying a body force **(b)** Body force starting to act **(c)** Reaching fully developed flow

Figure 12: Velocity profile transition

3.2 Spring Network

Trypanosoma cruzi bloodstream form is modeled by mixing knowledge-based approach with physics principles. Parasite shape was obtained by processing recordings from [29].

After setting up nodes' initial positions and mass, connection points were defined and linked by springs in order to preserve whole body area as well as forces and momentum equilibrium at every point [38]. An example of spring network cell body is depicted in13:

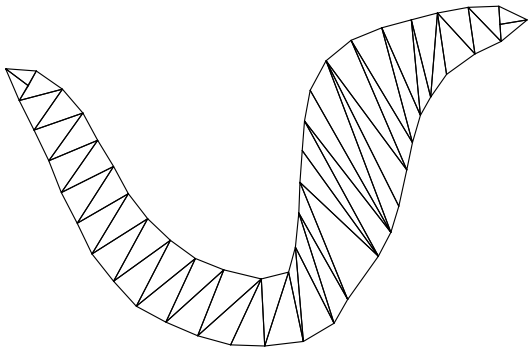

Figure 13: Bloodstream trypomastigote structure without flagellum.

For the ease of testing, an alternative and simpler structure was created, it is illustrated in 14:

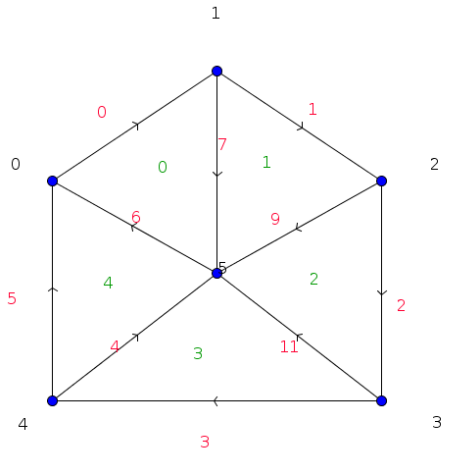

Figure 14: Test structure.

In both cases, structure edge nodes as well as triangle nodes were numbered in clockwise direction [16]. Since nodes were associated to triangles with a mesh generator [75] it was necessary to renumber the nodes after identifying if the position of one with respect to another was clockwise or counterclockwise. Such identification was done by means of the signed area of each triangle, it is using half the determinant of the matrix of distances from node i to node j and from node j to node k,:

$$A = \frac{1}{2} \det \begin{vmatrix} \vec{U}_{ij} \\ \vec{V}_{jk} \end{vmatrix} \tag{14}$$

$$Direction = \begin{cases} \text{Counterclockwise}, & \text{if } A > 0 \\ \text{clockwise}, & \text{if } A < 0 \end{cases}$$

Using a recording of the parasite, available in [29], its motility was discretize with five structures that implicitly include the effect of flagellar beating. The motion discretizations and its correspondent triangulations are presented in[Tab. 5]:

Discretization	Triangular mesh representation
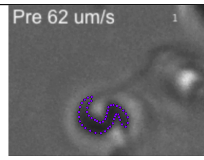	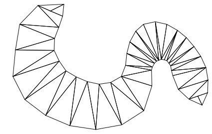
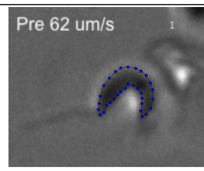	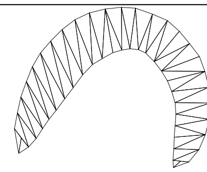
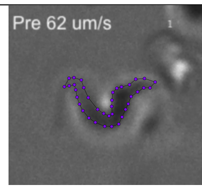	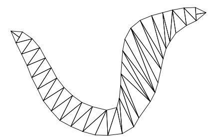
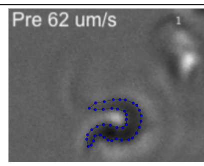	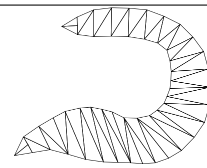
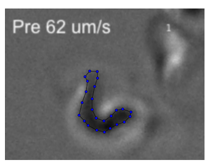	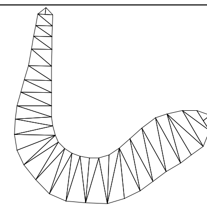

Table 5: Cellular motion discretization and triangle mesh representing it.

The mesh generator [75] used to triangulate the discretizations guarantees they are Delaunay, which is important to avoid acute angles and, in consequence, rounding errors. The distributions of the triangles areas are:

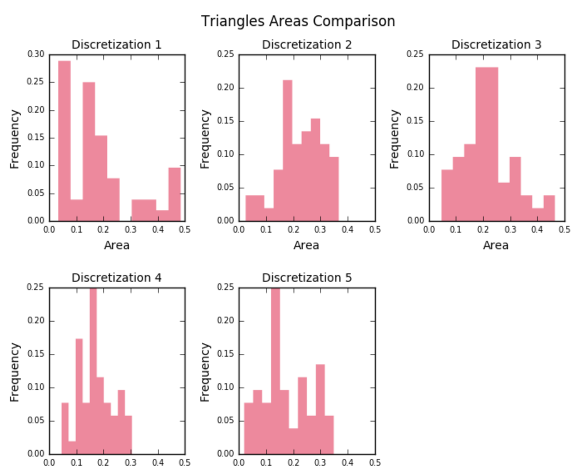

Figure 15: Distribution of the triangles areas in discretizations

Once the meshes were created, length was measured for all of them [Tab. 6]:

Discretization	Upper	Lower
1	8.7179	10.6343
2	12.4529	9.58477
3	11.4621	12.0608
4	11.5677	8.78758
5	8.46291	10.8171

Table 6: Discretizations length for upper and lower borders of cell membrane

Then,the discretizations areas were compared -taking the first one of them as reference [Tab. 7]. Although some differences were found they were considered to be expected since we are dealing with a biological structure flexible enough to pass through capillaries.

	Discretization				
	1	**2**	**3**	**4**	**5**
Total Area	9.316533	11.731044	11.207068	8.939633	9.183640
Area Change		+25.916%	+20.292%	-4.045%	-1.426%

Table 7: Discretizations area comparison

To preserve the discretizations stable, we have defined two constraints, one for the area and another for the angles. They are described below:

3.2.1 Area Preservation Constraint

Since parasite structure is exposed to forces resulting from the interaction with flow particles, a force to preserve triangles local area and global area as well must be exerted. A coefficient related with the hydrostatic elastic energy is calculated for each triangle as in [28]:

$$\alpha = -k_d \frac{(A_k - A_0)}{4A_0A_k} \tag{15}$$

Then, it is used to generate forces to be applied at each triangle node as follow:

$$\begin{aligned} Fn_i &= \alpha(\vec{\xi} \times \vec{a}_{kj}) \\ Fn_j &= \alpha(\vec{\xi} \times \vec{a}_{ik}) \\ Fn_k &= \alpha(\vec{\xi} \times \vec{a}_{ji}) \end{aligned} \tag{16}$$

Where $\vec{\xi}$ is the cross product between $\vec{a}_{ji}$ and $\vec{a}_{ik}$.

3.2.2 Angle Preservation Constraint

Conservation of structure area is important but by itself such constraint is unable to preserve the parasite shape. In order to do so the angles of each triangle must be maintained. This leads to apply over the nodes, a force proportional to the angle change:

$$F_\theta = -\frac{1}{2}\Delta\theta k_\theta \tag{17}$$

$\Delta\ \theta$ denotes the difference between instantaneous angle (θ_t) at time step t and spontaneous angle (θ_0) while k_θ is the angle constraint constant. Once the magnitude of the angle force (F_θ) is calculated, it is distributed between

the correspondent nodes.
For instance, if the angle is located at node k the resulting update in nodal forces (Fn) would have an effect on nodes i and j as follows:

$$\begin{aligned} Fn'_i &= Fn_i + F_{\theta_k} Tn_{ki} \times \hat{Z} \\ Fn'_j &= Fn_j + F_{\theta_k} Tn_{kj} \times -\hat{Z} \end{aligned} \tag{18}$$

Here $\hat{Z}$ is the triangle normal.

3.2.3 Cell body motility

Parasite motility results from the combination of internal and external forces, the first due to the transition between parasite motion discretizations and the second corresponds to the force exerted by the flow. The effect of the external forces will be explained in next section.
Having all the discretizations properly triangulated, parasite motion was induced by updating the natural length (l_0) of all springs, initial area (a_0) of all triangles, and the initial angles (θ_0) within the triangles of current structure, with data of a destination structure. After doing so, constraints associated forces act freely.

Once all motility contributions are taken into account, the network nodes position are updated and the process repeated during a prescribed number of time steps (Δt).

3.3 Collisions

This section presents the integration of the spring network model and the dissipative particle dynamics model. At this point the disposition of the nodes over the cell membrane becomes relevant, as was already stated the nodes were ordered in clockwise direction and this ensures that in every case the momentum vector from one node to another points out of the cell membrane. This can be achieved through the cross product between the momentum vector and the unit vector of the Z axis.
For instance, let $\widehat{Tn}_{ij}$ be the vector pointing in clockwise direction from node i towards node j at triangle n, then we get:

$$\begin{aligned} \widehat{Tn}_{ij} &= (Tn_{xi-xj}, Tn_{yi-yj}, Tn_{zi-zj}) \\ \widehat{Tn}_{ij} \times \hat{Z} &= \hat{x}(Tn_{yi-yj} - 0) + \hat{y}(0 - Tn_{xi-xj}) + \hat{z}(0 - 0) \end{aligned} \tag{19}$$

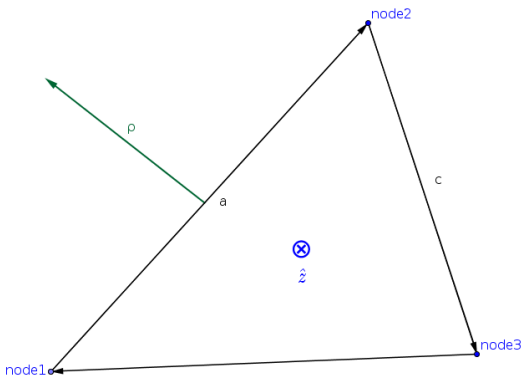

Figure 16: Momentum vector pointing out of the structure.

This vector $\vec{\rho}$ plays a key role on the integrated performance of the models as it is used to keep particles out of the structure, a detailed explanation is presented below.

3.3.1 Bounce back

Given each triangle springs length, nodes positions and its vectors pointing out, the dot product of the latter with each fluid particle vector of distances to triangle nodes is calculated to identify if such vectors are parallel and its directions are the same or not. Opposite directions will lead to mark a particle as crossing structure limits.

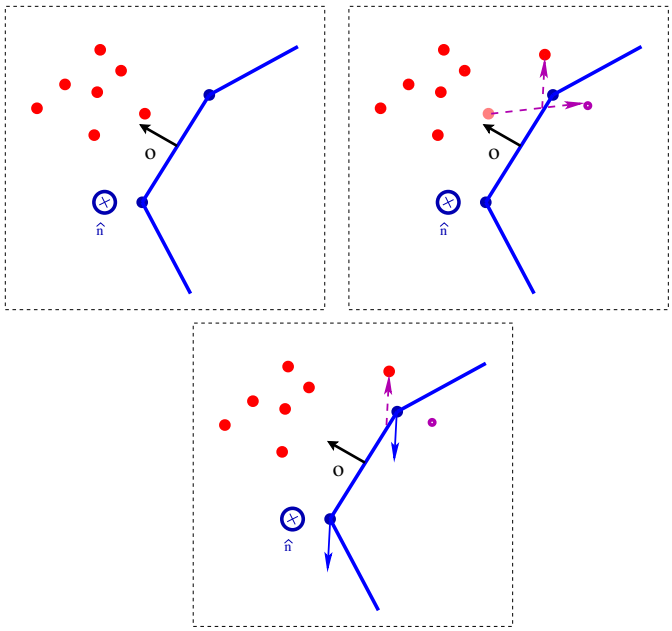

Figure 17: Group of fluid particles approaching to cell membrane.

Once a particle is detected crossing the structure limits its relative position to the outermost node is calculated and a force is derived from it as follows:

$$r_{dpd-n} = r_{dpd} - r_n \tag{20}$$

$$\iota = r_{dpd-n} \times \vec{\rho} \tag{21}$$

$$\Delta F_\iota = \iota \times \kappa \times \vec{\rho} \tag{22}$$

$$\Delta\rho = \Delta F_\iota \times \Delta t \tag{23}$$

Where ι measures how much a particle crossed the limits of the structure, κ is a coefficient relative to the strength of the interaction between the fluid and the cell membrane, Δt is the time step, and ΔF and $\Delta\rho$ are the changes on the force and momentum respectively.

Every particle passing through the structure gets an update on its position in response to momentum change in the perpendicular direction:

$$\rho'_{dpd} = \rho_{dpd} + \Delta\rho \tag{24}$$

The change on momentum ($\Delta\rho$) is also transferred to the triangle nodes taking part in the interaction in the form of a force:

$$
\begin{aligned}
Fn'_i &= Fn_i + \frac{1}{2}\frac{\Delta\rho}{\Delta t} \\
Fn'_j &= Fn_j + \frac{1}{2}\frac{\Delta\rho}{\Delta t}
\end{aligned}
\tag{25}
$$

In 24 and 26 ρ'_{dpd} are the updated momentum of a DPD particle and Fn' the updated force over nodes i and j.

3.4 Model Units

While the model internal units are needed to parametrize the real system into the simulation, not all the information is available. Therefore some of the values have to be estimated from the images, others can be freely choosen, and finally a third set of values would depend of those first two sets and therefore have to be calculated. Model length unit l is therefore arbitrarily defined by setting the equivalence between one internal unit and the distance in the real blood vessel as $[\ l\ ] = 1\ [\mu m]$.

To characterize the parasite mass, we took one snapshot of the videos [29], discretized the parasite, and measured its area and length; as well as the fluid area around it. This gives a sample simulation box, with the parameters (in internal units) as summarized in 8.

Physical Property	**Parasite**	**Flow**
Length	19.3963*	45
Mass	40.9019	9000
Area	9.31653*	540

Table 8: Simulation units - *Properties measured in the reference discretization

The internal units for each fluid particle mass (m_f) and the time step (δt) are given the values of ten and 5×10^{-4} respectively. Blood density is equal to $1.025 g/cm^3$ so the amount of mass in one (μm^2) of fluid, v_f, assuming depth contribution to volume is equal to the unit, comes to be:

$$
\begin{aligned}
\frac{v_f}{\mu m^2} &= \frac{1.025 g}{cm^2} \\
v_f &= 1.0250 \times 10^1 \,\mathrm{ng}
\end{aligned}
\tag{26}
$$

For a channel with an area (A_f) equal to $540 \mu m^2$ the total fluid mass in it is:

$$
\begin{aligned}
m_f &= v_f A_f \\
m_f &= 5.5350 \,\mu\mathrm{g}
\end{aligned}
\tag{27}
$$

There is no report of the parasite mass in literature so to overcome this lack of information we take as reference the measurements of cell density for erythrocytes[30], human lung cancer cells, and mouse lymphoblastic leukemia cells [12], which in all mentioned cases is close to $1 g/cm^3$, so it was assumed that cell body density of the parasite is at least equal to that of the water. Since the model is a two-dimensional representation, density is given as grams per unit of area, (ρ_{A_c}): $1 g/cm^2$. As reported in [Tab. 3] parasite dimensions vary within a range so the estimated mass per area (A_c) has the following boundaries:

$$
\begin{aligned}
m_c &= A_c \cdot \rho_{A_c} \\
m_{c-min} &= 12\,\mu\text{m}^2 \cdot 1\,\frac{\text{g}}{\text{cm}^2} = 1.2000 \times 10^{-7}\,\text{g} \\
m_{c-max} &= 52\,\mu\text{m}^2 \cdot 1\,\frac{\text{g}}{\text{cm}^2} = 5.2000 \times 10^{-7}\,\text{g}
\end{aligned} \tag{28}
$$

The scale units are the result of the relation between the physical system units (denoted with $'$) and the model units as follows:

$$M_0 = \frac{m'}{m} \tag{29}$$

$$T_0 = \frac{t'}{\delta t} \tag{30}$$

$$R_0 = \frac{r'}{r} \tag{31}$$

$$PA_0 = \frac{\rho A'}{\rho A} \tag{32}$$

Where M_0,T_0,R_0,and PA_0 are mass, time, length, and area density respectively.
With the preceding definition and taking into account that in the recording[29] the transition from discretization one to five takes 91 $[cs]$, the equations from (29) to (32) were used to calculate the basic units scale factors between the physical system and the simulation:

$$
\begin{aligned}
M_0 &= \frac{5.5350}{9000}\,\mu\text{g} = 6.1500 \times 10^{-1}\,\text{ng} \\
T_0 &= \frac{91}{500} cs = 1.8200 \times 10^{-3}\,\text{s} \\
R_0 &= 1\,\mu\text{m} \\
PA_0 &= \frac{1.0250}{1.6667 \times 10^{1}}\,\frac{\text{g}}{\text{cm}^2} = 6.1500 \times 10^{-2}\,\frac{\text{g}}{\text{cm}^2}
\end{aligned}
$$

About area density it is worth to mention that the ratio between the parasite and fluid, it is 1:1.025, from the real system was preserved in the simulation.

By using the previously obtained scale factors, velocity (V_0) and acceleration (a_0) were derived:

$$
\begin{aligned}
V_0 &= \frac{R_0}{T_0} = \frac{1}{1.8200 \times 10^{-3}}\,\frac{\mu\text{m}}{\text{s}} = 5.4945 \times 10^{-2}\,\frac{\text{cm}}{\text{s}} \\
a_0 &= \frac{R_0}{T_0^2} = \frac{1}{3.3124 \times 10^{-2}}\,\frac{\mu\text{m}}{\text{s}^2} = 3.0190 \times 10^{1}\,\frac{\text{cm}}{\text{s}^2}
\end{aligned} \tag{33}
$$

3.4.1 Parasite mass

Mass is distributed equitatively along the cellular body, being N_n the amount of nodes, m_n each node mass, A_{Tc} the parasite area, and ρA_c, its area density:

$$m_n N_n = \rho A_c A_{Tc} \tag{34}$$

Triangles are linked through 54 nodes and since the parasite's estimated area is approximately $32\mu m^2$ [Tab. 3], each node mass m_n comes to be:

$$
\begin{aligned}
m_n &= \frac{\rho A_c A_{Tc}}{N_n} \\
m_n &= \frac{1\,\frac{\mathrm{g}}{\mathrm{m}^{-4}} \cdot 32 m^{-12}}{54} \\
m_n &= 5.9259\,\mathrm{ng}
\end{aligned}
$$

3.4.2 Reynolds number

Reynolds number was obtained by following the approach proposed by Backer[5] based on the velocity of the system:

$$\langle V_x \rangle = \frac{\rho g_x D^2}{12\eta} \tag{35}$$

Where ρ is the system mass density which is assumed to remain constant during the simulation, g_x is the external force applied to the particles,η is the system dynamic viscosity, D is half the length of the system box, and V_x is the particles velocity measured parallel to g_x.

Given the expression (36):

$$Re = \frac{\rho \langle V_x \rangle D}{\eta} \tag{36}$$

Isolating η from (35) to replace it in (36) allows to calculate the Reynolds number in the simulation as:

$$Re = \frac{12\langle V_x^2 \rangle}{g_x D} \tag{37}$$

Now, by using the scale factors previously calculated in (33) we obtained that the scale factor to get the Reynolds number for the physical system is the unit:

$$
\begin{aligned}
Re_0 &= \frac{\left(5.4945 \times 10^{-2}\,\frac{\mathrm{cm}}{\mathrm{s}}\right)^2}{3.0190 \times 10^{1}\,\frac{\mathrm{cm}}{\mathrm{s}^2} \cdot 1 \times 10^{-4}\,\mathrm{cm}} \\
Re_0 &= 1.0000
\end{aligned} \tag{38}
$$

4 RESULTS

In this section we present the results of a coupled simulation, the flow produced with the DPD particles and the parasite structure were integrated to retrieve measurements of the *T. cruzi*'s bloodstream trypomastigote mechanical properties.

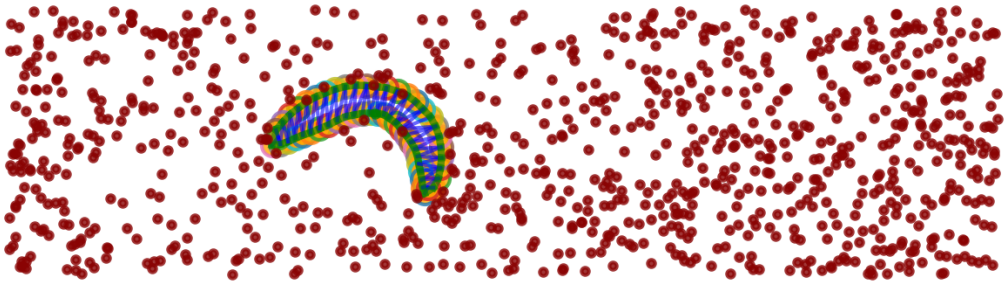

Figure 18: Coupled simulation

Base case measurements correspond to those from the structure in the pressence of the fluid but with no flow at all, it is, $Re \approx 0$. We also configured the flow to reach Reynolds numbers close to those from the heart, oesophagus, and colon since those are the most relevant parasitized organs in the human body. The set of experiments consist on two channels with different flow directions (parallel and perpendicular to the parasite's horizontal axis), for each one of them we performed three replications per organ using different seeds to initialize the particles position.

In all cases the simulation time was $1e6$ internal units, we used a channel of 45 µm length by 12 µm height and applied periodic boundary conditions on left and right sides of the channel for the base case and parallel flows simulations, for the perpendicular flows the periodic boundary conditions worked on the upper and bottom ends. The external force applied to induce the flow was 0.055. A complete migration, it means from first to last discretization, requires five hundred thousand time steps.

To keep the Reynolds numbers in the ranges of interest, we set a limit on the maximum velocity the flow could reach. The list of values and the average Reynolds numbers obtained in the simulations are in 9:

		Average Reynolds number	
	Limit velocity	**Parallel Flow**	**Perpendicular Flow**
Heart	1.4	144.0200	178.8087
Oesophagus	2.9	605.4840	679.9573
Colon	4.0	1146.1113	1202.1363

Table 9: Set of limit velocities and Reynolds numbers obtained

We compared the simulations based on cell deformation, energy, and displacement.

4.1 Cell Deformation

Cell interaction with the environment is a complex process because it occurs at both physical and biochemical levels, the response of the cell to external mechanical stimuli triggers intracellular activity in a process that has been called mechanotransduction [6]. In that matter, researchers have found, for instance, that cell elongation occurs as an adaptive response to changes in the availability of nutrients in the environment and could trigger *T. cruzi* metacyclogenesis [85] but elongation can also be induced by the flow, as reported for red blood cells [[84], [59]] or endothelial cells [49].

Cell deformation is a process that can be either reversible or permanent and several factors like cell viscoelasticity, viscoplasticity, cell geometry or the time scale during which the stimulus is applied play an important role in the outcome [57]. It continues to be intensively studied, among others, in search of understanding the contribution of stiffed red blood cells to changes in blood viscosity[[26],[77]], the hydraulic fracture of epithelial clusters [13], as a biomarker in breast cancer [37], its importance during macrophage inflammatory response [65], and to explain functions like cell adhesion under shear flow, as reported in [66].

Unfortunately *T. cruzi* is not yet part of the main focus of cell deformation research, in consequence there is a lack of studies on the mechanical interaction between the parasite membrane and the blood flow. The mentioned research gap forced us to define and tune κ in 22. The coupled model is sensitive to the interaction strength and major changes on this coefficient could lead to biologically unfeasible values of forces and, in consequence, loss of the structure shape.
Here, we found after coupling the models that the structure presents minor changes on its end-to-end distance 10 in response to different Reynolds numbers, in all cases those changes were reversible:

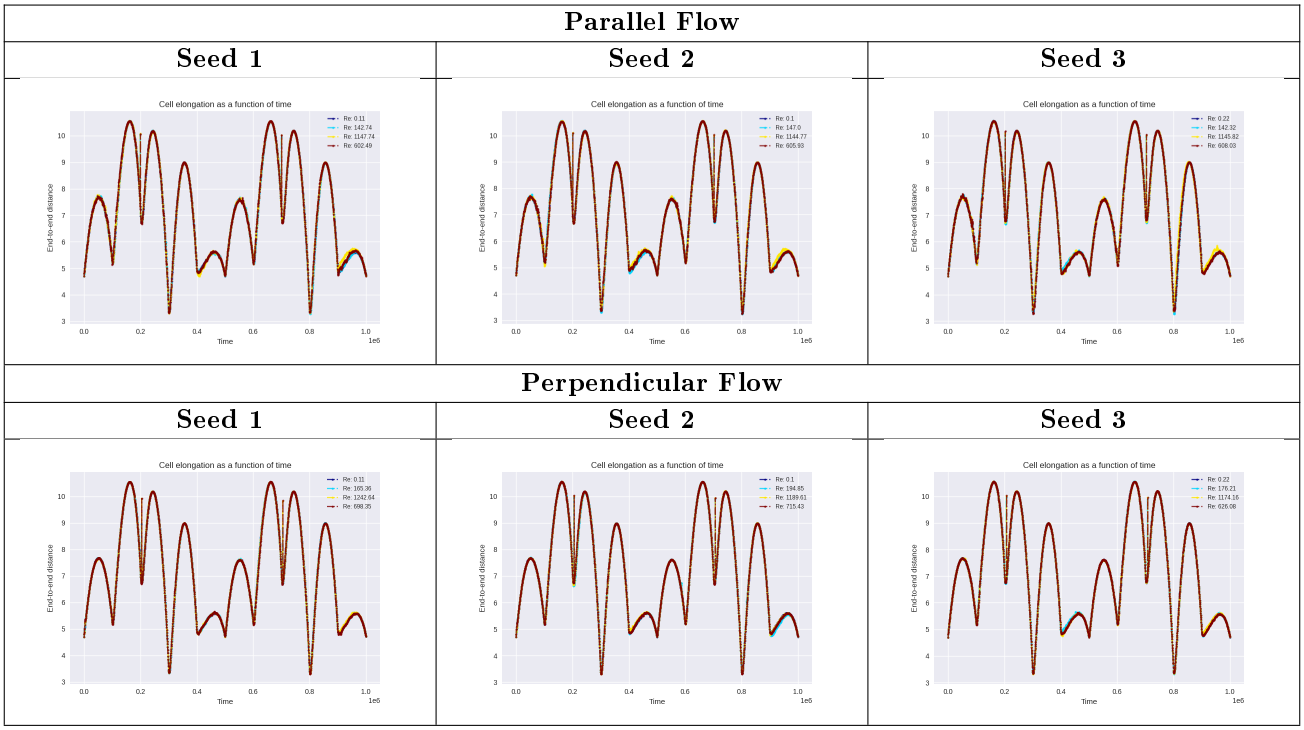

Table 10: Effect of the flow on parasite elongation

The cyclical behaviour of the results indicates that regardless of the flow conditions it is exposed to, the structure continuously reaches the predefined equilibrium configurations once all internal and external forces act.

We studied changes in cell elongation at the local level as well. Throughout the simulation, we measured the angle formed by the vector pointing from the centroid of a chosen triangle to its first node and the axis on which the external force applied to produce the flow acts. The orientation of a particular triangle within the triangulation is used as a proxy of the orientation of the system as a whole. In 11, we present the difference between the angle measured in base case simulations and that measured in each of the flows.

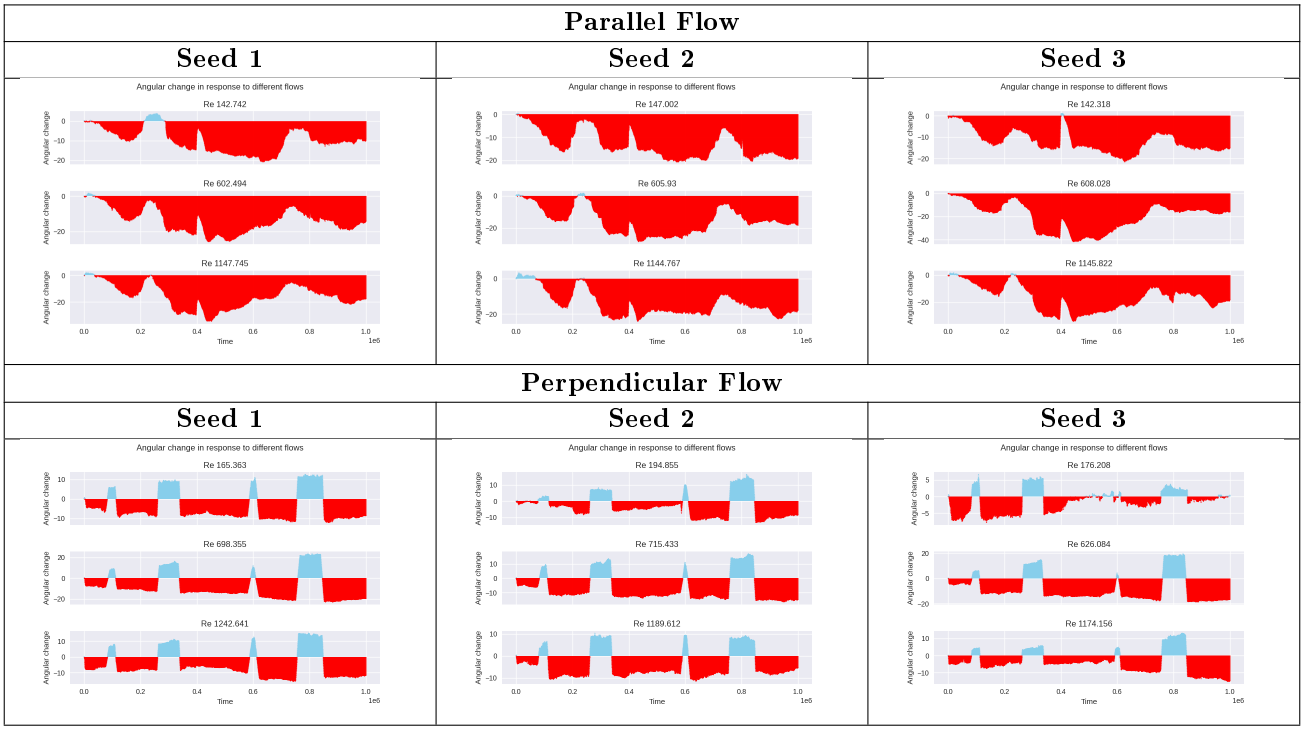

Table 11: Angular change in response to different flow conditions

For the parallel flows, we found the expansion of the triangle is the predominant behaviour, under the effect of vertical flows the triangle switches between contraction and expansion. The main difference between the flows of each set of experiments lies in the magnitude of the change experienced by the structure, but such results cannot be attributed to the magnitude of the Reynolds number.

Compared to the base case, larger Reynolds numbers demand more work from the structure to preserve its shape via the local level constraints. Which, in turn, have shown to be enough to preserve global structure length and area as presented in 7.
After comparing the results from the different Reynolds numbers, we couldn't identify a correlation between the flow and the structure response.

Our results are consistent with [86] where experiments with live cells demonstrated that cell elongation has little dependence on flow velocity. We consider that the small effect of the forces over the cell structure is an indicator of the reduced deformability of the parasitic cell.

4.2 Energies

Adenosine-triphosphate (ATP) is a molecule present in all the living forms given its task as energy carrier, cells have a wide variety of mechanisms for ATP synthesis as well as to convert chemical energy into mechanical work [41]. Flagellated swimmers, like *T. cruzi*, hydroliyze ATP in the axenome to produce motion, in [15], researchers found a linear relationship between ATP expenditure and flagellar beating.

We focus on measuring the energy demanded by the structure to produce what we have defined as its natural motion under different flow conditions. The evolution of kinetic and potential energy for the first seeds are presented in 12, the results obtained for the remaining experiments are in the APPENDIX.
The amount of energy stored by the structure increases in response to the induced migration between discretizations and, once all the updates described in 3.2.3 take place, the transition starts.

<table>
<tr><th colspan="2">Parallel Flow - Seed 1</th></tr>
<tr><th>Base Case</th><th>Heart</th></tr>
<tr><td> 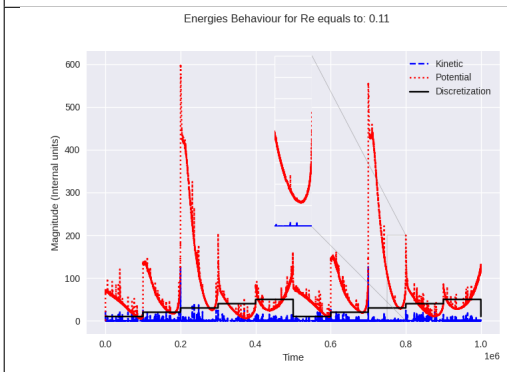
</td><td> 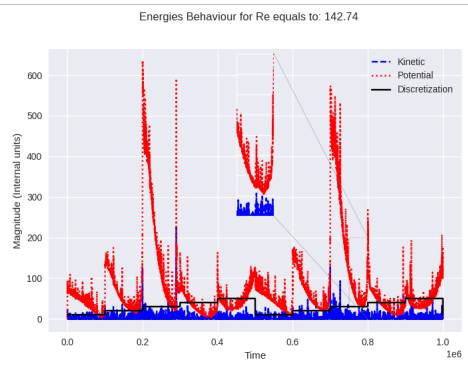
</td></tr>
<tr><th>Oesophagus</th><th>Colon</th></tr>
<tr><td> 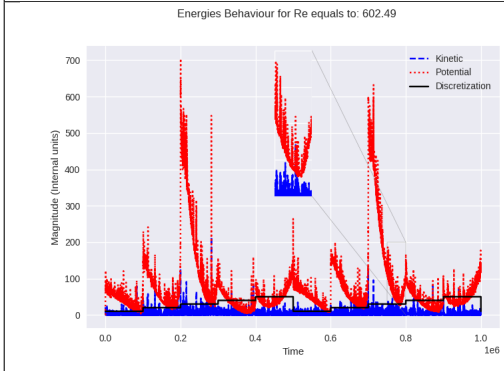
</td><td> 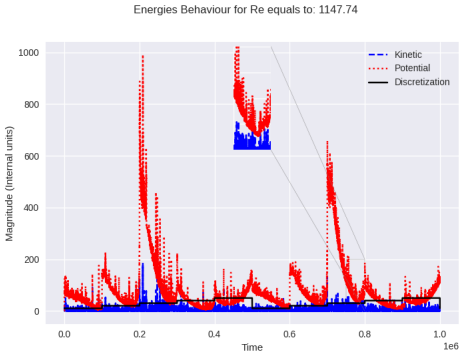
</td></tr>
<tr><th colspan="2">Perpendicular Flow - Seed 1</th></tr>
<tr><th>Base Case</th><th>Heart</th></tr>
<tr><td> 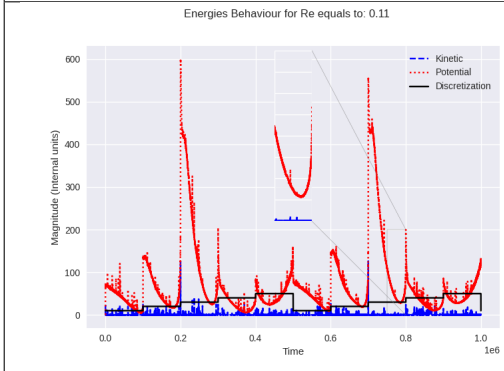
</td><td> 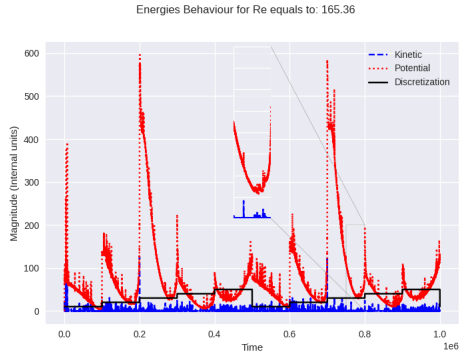
</td></tr>
<tr><th>Oesophagus</th><th>Colon</th></tr>
<tr><td> 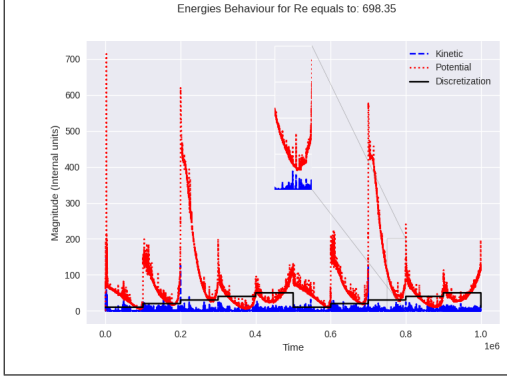
</td><td> 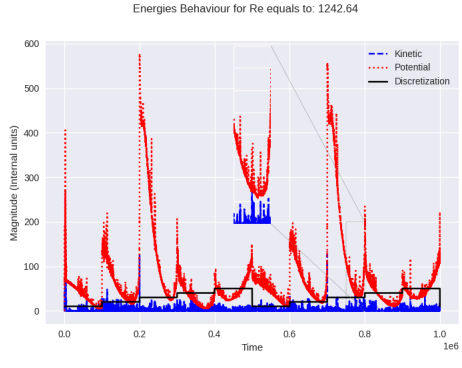
</td></tr>
</table>

Table 12: Energies behaviour as a function of time - Seed 1

4.2.1 Potential Energy

During the transition between discretizations the structure begins to consume potential energy, and this approaches zero as the next steady state is reached 12. We found variations in potential energy magnitude between the parallel flows and small changes when it comes to perpendicular flows.
Once we compared the first three experiments of each seed from the parallel flows, we found the change on the medians appears to be proportional to the Reynolds numbers. However, this trend is lost when we bring the results of the colon flows into the analysis because its medians are close -even minor- to those of the oesophagus experiments. Such a situation could perhaps be an indication that for this particular model there is a limit on the potential energy, and it is close to being reached.

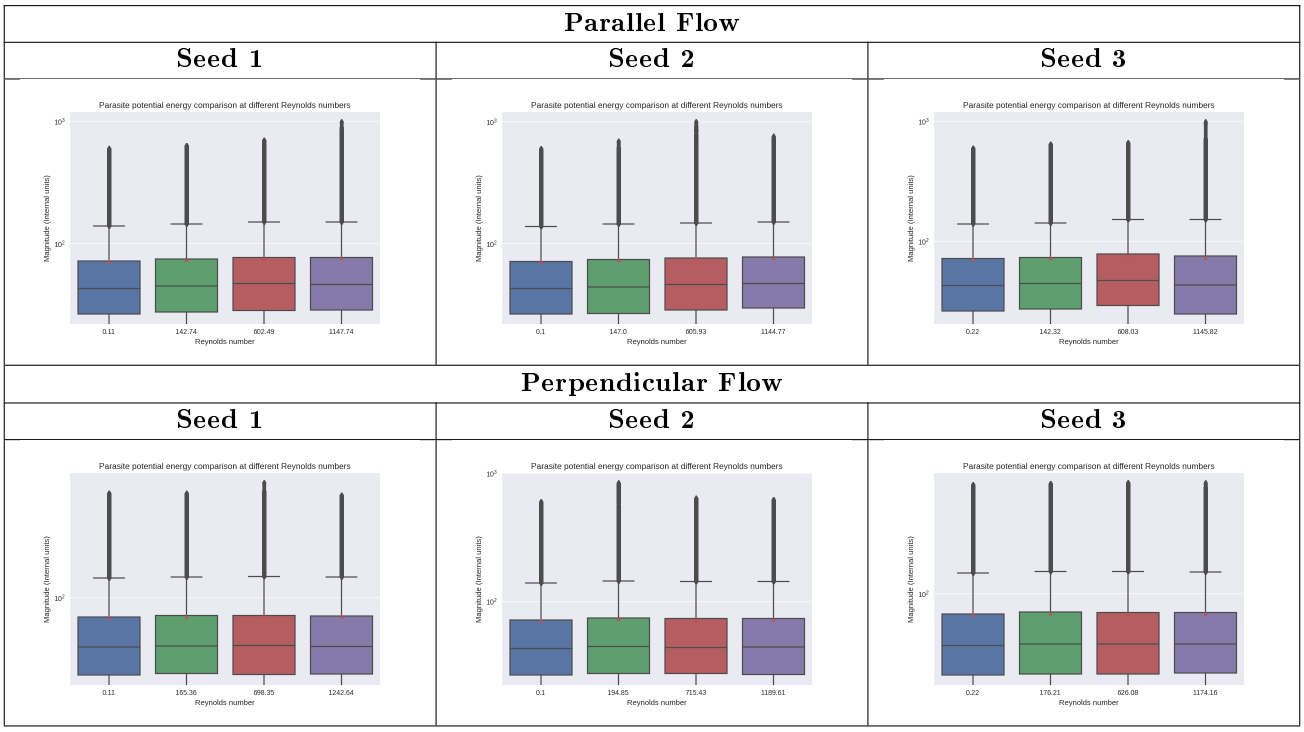

Table 13: Parasite potential energy in response to different flows

The distribution of the potential energy for the perpendicular flows is almost exactly the same in all cases and this allows us to think in flow orientation as a determinant factor in the cell-flow interaction.
We also observed that although larger amounts of energy are available, the interaction with the fluid also demands the structure to increase energy consumption, explaining why the distribution of the energy across the entire set of experiments is similar. This can be supported by:

1. The fact that the potential energy still reaches minimum values before a new transition begins 12.
2. The relative closeness between the medians and the interquartile ranges in 13.

4.2.2 Kinetic Energy

In 12 we found evidence of flow-induced changes in the kinetic energy of the parasite. As oppossed to the potential energy, in all the experiments the magnitude of kinetic energy and the Reynolds number are clearly correlated, and once again, the effect of the perpendicular flows is the smallest. This is confirmed in 14 because the interquartile ranges of the perpendicular flows remain not only close to the base case simulation but in the same order of magnitude, whilst in the perpendicular flows experiments the median rapidly increases and the upper limit of the interquartile range is one order of magnitude higher than that of the reference experiment.

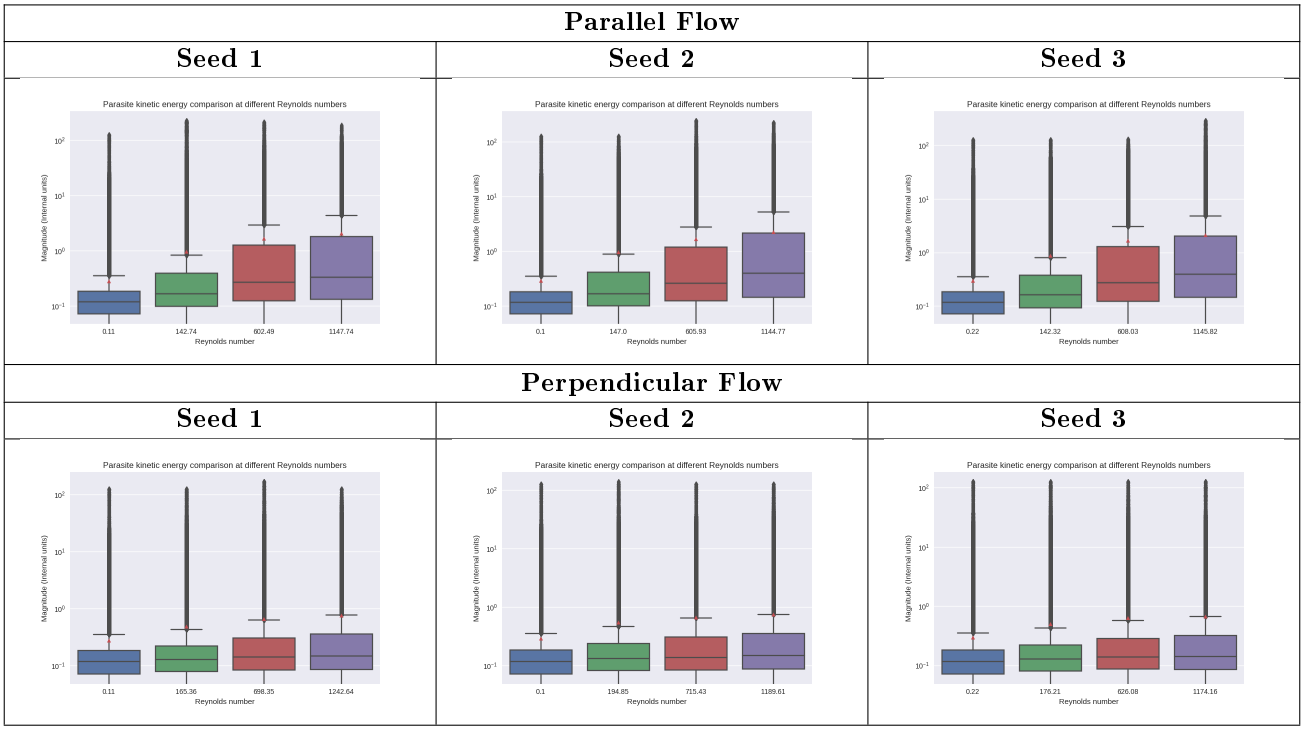

Table 14: Parasite kinetic energy in response to different flows

In [51], metacyclic trypomastigotes from CL and G strains were put into starvation after reducing the availability of ATP. This resulted in depleted infectivity rates and demonstrating cell invasion is a process that, independent of the strain-specific engaging strategies, demands the cell to invest energy for its completion. In light of our results, parasite motility is affected by the flow because the energy expenditure to perform it rises when the flow velocity does. Given the increase in energy needs, one might think of flows characterized with high Reynolds numbers as hostile to the main processes leading to parasite proliferation: motion and cell invasion.

But the reality of the disease is that even under such harsh conditions the infection can reach advanced stages, so our findings seem to be the losing side of an emerging trade-off. In order to understand what possibly the gains for the parasite are, some questions and facts arise:

1. Are those enviroments populated with more cells susceptible of being parasitized by *T. cruzi*?
2. The appearance of nanotubes in the flagellum has been reported as a possible mechanism to improve cell adhesion when the *T. cruzi* epimatigotes face shear flows [66], does the trypomastigote possess a similar mechanism to adhere and eventually cause damage to the host's cells?
3. Cell damage causes an increase in the available amount of extracellular Adenosine-triphosphate (eATP). eATP is used for cell-to-cell communication and is recognized as a trigger of the inflammatory response [83], it is also known that trypomastigotes are able to hydrolyze eATP [55].

We speculate that in a rich environment with improved cell adhesion, the parasite can harm more cells, causing the amount of eATP to surge without the risk of strong activation of the immune system. The mentioned risk is considered to be reduced if the parasite consumes the eATP to compensate the additional amount of energy demanded during the interaction with the surrounding flow.

4.3 Center of Mass

Motility is relevant during the entire life cycle of the parasite because it takes part in several processes including cell development, adhesion to host cells, and the evasion of the immune system. For kinetoplastids as *T. cruzi*, the dynein motor proteins in the axenome are responsible for providing the force needed to produce flagellar beating[43].

Our spring network model does not explicitly represent the flagellum because we consider its effect is already part of the resulting discretizations, to us, this assumption helps to simplify the model and is safe for two reasons:

1. *T. cruzi* swimming is the result of global changes in cell shape as a consequence of the flagellum being attached to the cell body [72], for this model a global change is represented by the transition between discretizations.
2. At the parasite level the inertial forces are neglected, leading to dominance of the viscous forces. In this scenario, the only way to produce displacement is non-reciprocal movement [35].

We found the motion discretization strategy 5 is close enough to the definition of non-reciprocal movement:"*a series of motions, wherein multiple parts are moved in* ***a specific order to cycle through fixed poses****. Reversing the order of motions would result in a different series of poses*"[3] as to guarantee displacement of the cell body.

To assess the effect of the flow on the parasite trajectory we tracked its center of mass during the simulations 15 and found the following:

1. For the parallel flows, we found that the structure is not only dragged by the flow but also that the difference with what we have referenced as the natural trajectory of the parasite is proportional to the magnitude of the Reynolds number.
2. On the other hand, perpendicular flow simulations show changes in the center of mass trajectory as well, but without a clear relationship with the Reynolds number. In fact, it seems that a flow perpendicular to the cell structure's horizontal axis exerts little effect over its trajectory, and this could be explained by parasite morphology or be the result of the channel configuration.

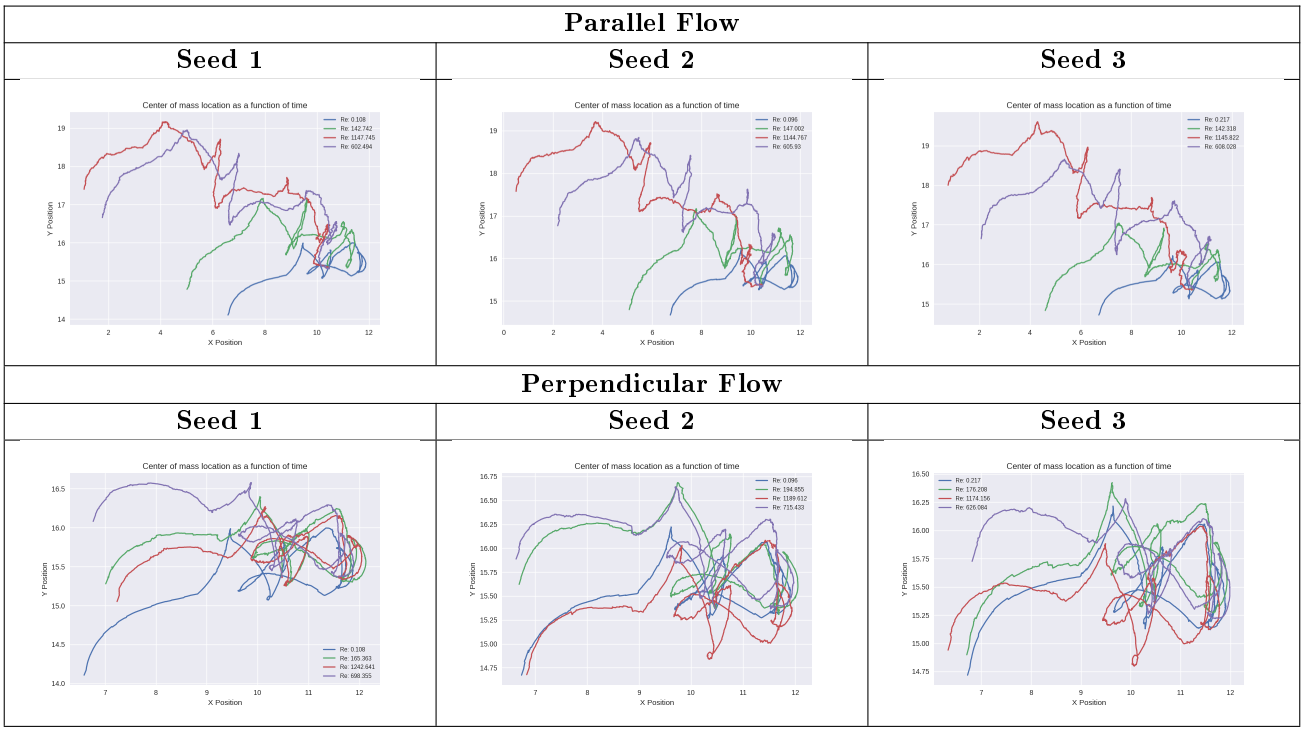

Table 15: Effect of the flow on parasite trajectory

Our findings are in partial agreement with the results from [86], exposing the structure to parallel flows resulted on the parasite displacing faster -as expected for a stiffer structure- and upstream in some kind of wavy trajectory. On the contrary, the perpendicular flows show the cell has no preferred direction of motion.

Flows parallel to the cell elongation direction could explain, to some extent, how the parasite travels within the human body reaching organs far from the entry wound: taking advantage of the drag produced by the flow. It also

[3] A. Hochstetter and T. Pfohl, Trends Parasitol.531-541, 32,7 (2016)

seems that for low Reynolds numbers in flows parallel to the horizontal axis of the structure or flows perpendicular to the same axis of the parasite and regardless of the Reynolds number, the chemotaxis-driven motility could be facilitated.

5 CONCLUSIONS AND FURTHER RESEARCH

We successfully represented the infective form of the *T. cruzi* with a spring network model where a set of harmonic springs act as the cell membrane and the mass of the parasite is distributed alongside the structure, aggregated in rigid nodes. This approach can be replicated to model other forms of the parasite and even it could result in the first attempt on *T. cruzi* metacyclogenesis modeling since the final stage of the parasite can be considered as another discretization to reach. A non-critical change to the cell model is the addition of the flagellum in order to evaluate if variations on flagellar pocket position have incidence on cell motility. For this model we consider three improvements are of the outmost importance:

1. Develop a 3D model of the cell body.
2. To carry out efforts on image processing so retrieving data points from *in vitro* recordings can be automated and other cell stages modelled with ease.
3. Turn the rigid nodes into dissipative particles.

During the modelling phase of the cell body, we faced continuous limitations due to the lack of data on the physical properties of the parasite, such as length, width, height, mass, or bending rigidity. Many of these drawbacks were overcome with extensive parameter testing to stabilize the structure.

Our second goal was to model the blood flow and couple the models. Sticking to the formal definition what we modelled here is a fluid similar to blood plasma, it is so because our model does not include RBC which are the most abundant corpuscles in blood. We arrived at this decision because red blood cells cannot be parasitized by *T. cruzi* and erythrocites modelling has been the focus of intesive recent research, a statement that does not hold true for this parasite. The flow was modelled via DPD.

The velocity distribution of the particles in our implementation of DPD produced a good fit to a Maxwell-Boltzman distribution. In addition, the thermostat is in good agreement with the Fluctuation-Dissipation theorem. As part of the flow characterization we also implemented the Poiseuille method and found the velocity profile agrees with the fully developed flow assumption. The Poiseuille method implementation is intended to produce further advances in this research because it allows us to assess the effect of shear flows on the parasite cell. In the future, we expect the flow to be represented as a combination of the current blood plasma flow and RBC in three dimensions.

The coupled simulation here presented allows measuring the effect of different flow conditions not only on mechanical properties of the cell body like cell elongation or motility but, in addition, it provides some interesting insights on energy expenditure. Our current work can be extended to simulate multiple cells. It is also worth mentioning that the parameters are susceptible to be refined as new information on the parasite physical properties comes out.

The results we obtained from models coupling confirm that flows are unable to produce major or permanent changes on cell elongation. We also observed some motility patterns similar to those reported from *in vivo* experiments, the cases where our results diverge from the experimentalists findings will be a matter of further analysis, for instance, on the effect of the channel dimension or the parasite morphology and its relationship with the flow direction. The behaviour of the energy during cell-flow interaction led us to propose an emerging trade-off mechanism to understand how the parasite obtains the additional energy it needs to preserve motility and take advantage of the flow to proliferate. In our concept, the blood flow plays a key role on cellular tropism, either because it drags the trypomastigotes to environments where more resources are available or because it allows the parasite to drive its motion by the chemical signal of potential host cells.

This thesis has contributed to increase our understanding of *T. cruzi* dynamics when exposed to different flow conditions, it is our hope that this work helps to pave the way to foster mathematical modelling research in neglected diseases.

6 LIST OF PRESENTATIONS

1. Workshop: Mechanical Forces in Biology: Theory and Simulation (2019), A parasite's thoughts: What's it like to swim inside you? (Oral presentation), Universidad de Los Andes, Colombia.
2. School: Computer simulations of biological membranes & free energy calculations of biomolecular systems (2018), Spring Network Model of Trypanosoma Cruzi bloodstream trypomastigote (Poster), Universidad de Los Andes, Colombia.
3. V International Conference on Particle-Based Methods (2017), Trypanosoma cruzi swimming in shear flow (Oral presentation). Leibniz Universität Hannover, Germany.

References

[1] B. Alberts, D. Bray, J. Lewis, M. Raff, K. Roberts, J. D. Watson, and A. Grimstone. Molecular biology of the cell (3rd edn). *Trends in Biochemical Sciences*, 20(5):210–210, 1995.

[2] D. Alizadehrad, T. Krüger, M. Engstler, and H. Stark. Simulating the complex cell design of trypanosoma brucei and its motility. *PLoS Comput Biol*, 11(1):e1003967, 2015.

[3] L. O. Andrade, L. Galvão, M. d. N. S. Meirelles, E. Chiari, S. D. Pena, and A. M. Macedo. Differential tissue tropism of trypanosoma cruzi strains: an in vitro study. *Memorias do Instituto Oswaldo Cruz*, 105(6):834–837, 2010.

[4] N. Ashton. Physiology of red and white blood cells. *Anaesthesia & Intensive Care Medicine*, 6(14):261–266, 2013.

[5] J. Backer, C. Lowe, H. Hoefsloot, and P. Iedema. Poiseuille flow to measure the viscosity of particle model fluids. *The Journal of chemical physics*, 122(15):154503, 2005.

[6] D. L. Bader and M. M. Knight. Biomechanical analysis of structural deformation in living cells. *Medical & biological engineering & computing*, 46(10):951–963, 2008.

[7] J. E. Bennett, R. Dolin, and M. J. Blaser. *Principles and practice of infectious diseases*. Elsevier Health Sciences, 2014.

[8] H. Berra, E. Piaggio, S. Revelli, and A. Luquita. Blood viscosity changes in experimentally trypanosoma cruzi-infected rats. *Clinical hemorheology and microcirculation*, 32(3):175–182, 2005.

[9] M. Bessis. *Corpuscles*. Springer Science & Business Media, 1974.

[10] C. Bishop and D. M. Surgenor. *The red blood cell*. Academic Press, 1964.

[11] B. Blasi, A. D'Alessandro, N. Ramundo, and L. Zolla. Red blood cell storage and cell morphology. *Transfusion medicine*, 22(2):90–96, 2012.

[12] A. K. Bryan, V. C. Hecht, W. Shen, K. Payer, W. H. Grover, and S. R. Manalis. Measuring single cell mass, volume, and density with dual suspended microchannel resonators. *Lab on a Chip*, 14(3):569–576, 2014.

[13] L. Casares, R. Vincent, D. Zalvidea, N. Campillo, D. Navajas, M. Arroyo, and X. Trepat. Hydraulic fracture during epithelial stretching. *Nature materials*, 14(3):343–351, 2015.

[14] M. Castillo-Riquelme, F. Guhl, B. Turriago, N. Pinto, F. Rosas, M. F. Martínez, J. Fox-Rushby, C. Davies, and D. Campbell-Lendrum. The costs of preventing and treating chagas disease in colombia. *PLoS Negl Trop Dis*, 2(11):e336, 2008.

[15] D. T. Chen, M. Heymann, S. Fraden, D. Nicastro, and Z. Dogic. Atp consumption of eukaryotic flagella measured at a single-cell level. *Biophysical journal*, 109(12):2562–2573, 2015.

[16] W. E. Committee et al. Control of chagas disease. *World Health Organization technical report series*, 905:i, 2002.

[17] N. Cunha-e Silva, C. Sant'Anna, M. G. Pereira, I. Porto-Carreiro, A. L. Jeovanio, and W. de Souza. Reservosomes: multipurpose organelles? *Parasitology research*, 99(4):325–327, 2006.

[18] W. Curtin and H. Scher. Mechanics modeling using a spring network. *Journal of Materials Research*, 5(03):554–562, 1990.

[19] W. de Souza, T. M. U. de Carvalho, and E. S. Barrias. Review on trypanosoma cruzi: host cell interaction. *International journal of cell biology*, 2010, 2010.

[20] W. de Souza, C. Sant'Anna, and N. L. Cunha-e Silva. Electron microscopy and cytochemistry analysis of the endocytic pathway of pathogenic protozoa. *Progress in Histochemistry and Cytochemistry*, 44(2):67–124, 2009.

[21] D. Despommier, J. Karapelou, et al. Parasite life cycles. *Parasite life cycles.*, 1987.

[22] R. Docampo and S. N. Moreno. The acidocalcisome. *Molecular and biochemical parasitology*, 114(2):151–159, 2001.

[23] G. P. Downey, D. E. Doherty, B. Schwab, E. Elson, P. Henson, and G. Worthen. Retention of leukocytes in capillaries: role of cell size and deformability. *Journal of Applied Physiology*, 69(5):1767–1778, 1990.

[24] M. Esin, E. Pasternak, and A. Dyskin. Stability of 2d discrete mass-spring systems with negative stiffness springs. *physica status solidi (b)*, 2016.

[25] D. Fedosov, B. Caswell, S. Suresh, and G. Karniadakis. Quantifying the biophysical characteristics of plasmodium-falciparum-parasitized red blood cells in microcirculation. *Proceedings of the National Academy of Sciences*, 108(1):35–39, 2011.

[26] D. A. Fedosov. *Multiscale modeling of blood flow and soft matter*. Brown University, 2010.

[27] D. A. Fedosov, B. Caswell, and G. E. Karniadakis. Wall shear stress-based model for adhesive dynamics of red blood cells in malaria. *Biophysical journal*, 100(9):2084–2093, 2011.

[28] D. A. Fedosov, H. Lei, B. Caswell, S. Suresh, and G. E. Karniadakis. Multiscale modeling of red blood cell mechanics and blood flow in malaria. *PLoS Comput. Biol*, 7(12):e1002270, 2011.

[29] E. J. Finkelsztein, J. C. Diaz-Soto, J. C. Vargas-Zambrano, E. Suesca, F. Guzmán, M. C. López, M. C. Thomas, M. Forero-Shelton, A. Cuellar, C. J. Puerta, et al. Altering the motility of trypanosoma cruzi with rabbit polyclonal anti-peptide antibodies reduces infection to susceptible mammalian cells. *Experimental parasitology*, 150:36–43, 2015.

[30] W. H. Grover, A. K. Bryan, M. Diez-Silva, S. Suresh, J. M. Higgins, and S. R. Manalis. Measuring single-cell density. *Proceedings of the National Academy of Sciences*, 108(27):10992–10996, 2011.

[31] K. Gull. The cytoskeleton of trypanosomatid parasites. *Annual Reviews in Microbiology*, 53(1):629–655, 1999.

[32] A. A. Gusev. Finite element mapping for spring network representations of the mechanics of solids. *Physical review letters*, 93(3):034302, 2004.

[33] R. J. Hayes and C. J. Schofield. Estimación de las tasas de incidencia de infecciones y parasitosis crónicas a partir de la prevalencia: La enfermedad de chagas en américa latina. *Boletín de la Oficina Sanitaria Panamericana*, 108(4):308–316, 1990.

[34] C. Hoare, F. Wallace, et al. Developmental stages of trypanosomatid flagellates: a new terminology. *Nature*, 212:1385–6, 1966.

[35] A. Hochstetter and T. Pfohl. Motility, force generation, and energy consumption of unicellular parasites. *Trends in parasitology*, 32(7):531–541, 2016.

[36] P. Hoogerbrugge and J. Koelman. Simulating microscopic hydrodynamic phenomena with dissipative particle dynamics. *EPL (Europhysics Letters)*, 19(3):155, 1992.

[37] H. W. Hou, Q. Li, G. Lee, A. Kumar, C. Ong, and C. T. Lim. Deformability study of breast cancer cells using microfluidics. *Biomedical microdevices*, 11(3):557–564, 2009.

[38] A. Jagota and S. Bennison. Spring-network and finite-element models for elasticity and fracture. In *Nonlinearity and Breakdown in Soft Condensed Matter*, pages 186–201. Springer, 1994.

[39] A. M. Jansen, S. C. Xavier, and A. L. R. Roque. The multiple and complex and changeable scenarios of the trypanosoma cruzi transmission cycle in the sylvatic environment. *Acta tropica*, 2015.

[40] N. A. Khan. *Emerging protozoan pathogens*. Taylor & Francis, 2008.

[41] A. E. Knight and J. E. Molloy. Coupling atp hydrolysis to mechanical work. *Nature Cell Biology*, 1(4):E87–E89, 1999.

[42] M. Kong, Y. Wu, G. Li, and R. G. Larson. A bead-spring model for running and tumbling of flagellated swimmers: detailed predictions compared to experimental data for e. coli. *Soft matter*, 11(8):1572–1581, 2015.

[43] T. Krüger and M. Engstler. Flagellar motility in eukaryotic human parasites. In *Seminars in cell & developmental biology*, volume 46, pages 113–127. Elsevier, 2015.

[44] D. N. Ku. Blood flow in arteries. *Annual Review of Fluid Mechanics*, 29(1):399–434, 1997.

[45] P. Kundu, I. Cohen, and D. Dowling. *Fluid Mechanics*. Elsevier Science, 2015.

[46] E. Lauga and T. R. Powers. The hydrodynamics of swimming microorganisms. *Rep. Prog. Phys*, 72(096601):096601, 2009.

[47] B. Y. Lee, K. M. Bacon, M. E. Bottazzi, and P. J. Hotez. Global economic burden of chagas disease: a computational simulation model. *The Lancet infectious diseases*, 13(4):342–348, 2013.

[48] D. Lee and J. Chen. Numerical simulation of steady flow fields in a model of abdominal aorta with its peripheral branches. *Journal of Biomechanics*, 35(8):1115–1122, 2002.

[49] M. Levesque and R. Nerem. The elongation and orientation of cultured endothelial cells in response to shear stress. 1985.

[50] C. R. Marinho, D. Z. Bucci, M. L. Z. Dagli, K. R. Bastos, M. G. Grisotto, L. R. Sardinha, C. R. Baptista, C. P. Gonçalves, M. R. D. Lima, and J. M. Álvarez. Pathology affects different organs in two mouse strains chronically infected by a trypanosoma cruzi clone: a model for genetic studies of chagas' disease. *Infection and immunity*, 72(4):2350–2357, 2004.

[51] R. M. Martins, C. Covarrubias, R. G. Rojas, A. M. Silber, and N. Yoshida. Use of l-proline and atp production by trypanosoma cruzi metacyclic forms as requirements for host cell invasion. *Infection and Immunity*, 77(7):3023–3032, 2009.

[52] M. J. McConville, K. A. Mullin, S. C. Ilgoutz, and R. D. Teasdale. Secretory pathway of trypanosomatid parasites. *Microbiology and Molecular Biology Reviews*, 66(1):122–154, 2002.

[53] J. L. McWhirter, H. Noguchi, and G. Gompper. Flow-induced clustering and alignment of vesicles and red blood cells in microcapillaries. *Proceedings of the National Academy of Sciences*, 106(15):6039–6043, 2009.

[54] R. Melo and Z. Brener. Tissue tropism of different trypanosoma cruzi strains. *The Journal of parasitology*, pages 475–482, 1978.

[55] J. R. Meyer-Fernandes, J. Saad-Nehme, C. E. Peres-Sampaio, R. Belmont-Firpo, D. F. Bisaggio, L. C. Do Couto, A. L. Fonseca de Souza, A. H. Lopes, and T. Souto-Padron. A mg-dependent ecto-atpase is increased in the infective stages of trypanosoma cruzi. *Parasitology Research*, 93(1):41–50, 2004.

[56] K. Miranda, M. Benchimol, R. Docampo, and W. de Souza. The fine structure of acidocalcisomes in trypanosoma cruzi. *Parasitology research*, 86(5):373–384, 2000.

[57] K. Molnar and M. Labouesse. The plastic cell: mechanical deformation of cells and tissues. *Open Biology*, 11(2):210006, 2021.

[58] A. Moncayo and M. Ortiz Yanine. An update on chagas disease (human american trypanosomiasis). *Annals of Tropical Medicine & Parasitology*, 100(8):663–677, 2006.

[59] M. Nakamura, S. Bessho, and S. Wada. Spring-network-based model of a red blood cell for simulating mesoscopic blood flow. *International journal for numerical methods in biomedical engineering*, 29(1):114–128, 2013.

[60] P. Nikunen, M. Karttunen, and I. Vattulainen. How would you integrate the equations of motion in dissipative particle dynamics simulations? *Computer Physics Communications*, 153(3):407–423, 2003.

[61] N. Nogueira and Z. Cohn. Trypanosoma cruzi: mechanism of entry and intracellular fate in mammalian cells. *The Journal of experimental medicine*, 143(6):1402–1420, 1976.

[62] M. C. P. Nunes, W. Dones, C. A. Morillo, J. J. Encina, et al. Chagas disease: an overview of clinical and epidemiological aspects. *Journal of the American College of Cardiology*, 62(9):767–776, 2013.

[63] T. Omori, T. Ishikawa, D. Barthès-Biesel, A.-V. Salsac, J. Walter, Y. Imai, and T. Yamaguchi. Comparison between spring network models and continuum constitutive laws: Application to the large deformation of a capsule in shear flow. *Physical Review E*, 83(4):041918, 2011.

[64] W. H. Organization et al. Research priorities for chagas disease, human african trypanosomiasis and leishmaniasis. *World Health Organization technical report series*, (975):v, 2012.

[65] N. R. Patel, M. Bole, C. Chen, C. C. Hardin, A. T. Kho, J. Mih, L. Deng, J. Butler, D. Tschumperlin, J. J. Fredberg, et al. Cell elasticity determines macrophage function. 2012.

[66] C. D. Perdomo Gómez et al. Nanotúbulos en trypanosoma cruzi como mecanismo de resistencia al flujo. 2021.

[67] C. J. Perez, A. J. Lymbery, and R. A. Thompson. Reactivation of chagas disease: Implications for global health. *Trends in parasitology*, 2015.

[68] A. Prata. Clinical and epidemiological aspects of chagas disease. *The Lancet infectious diseases*, 1(2):92–100, 2001.

[69] A. Rassi and J. M. de Rezende. American trypanosomiasis (chagas disease). *Infectious disease clinics of North America*, 26(2):275–291, 2012.

[70] A. Rassi and J. A. Marin-Neto. Chagas disease. *The Lancet*, 375(9723):1388–1402, 2010.

[71] J. Rastetter. *Atlas of Clinical Hematology*. Number Ed. 6. Springer Science & Business Media, 2004.

[72] U. S. Schwarz. Physical constraints for pathogen movement. In *Seminars in cell & developmental biology*, volume 46, pages 82–90. Elsevier, 2015.

[73] S. Sell, E. E. Max, and I. Berkower. *Immunology, immunopathology and immunity*. ASM press Washington, DC, 2001.

[74] T. A. Shapiro and P. T. Englund. The structure and replication of kinetoplast dna. *Annual Reviews in Microbiology*, 49(1):117–143, 1995.

[75] J. R. Shewchuk. Triangle: Engineering a 2d quality mesh generator and delaunay triangulator. In *Applied computational geometry towards geometric engineering*, pages 203–222. Springer, 1996.

[76] M. A. Shikanai-Yasuda and N. B. Carvalho. Oral transmission of chagas disease. *Clinical Infectious Diseases*, page cir956, 2012.

[77] S. Shin, Y. Ku, M.-S. Park, and J.-S. Suh. Deformability of red blood cells: a determinant of blood viscosity. *Journal of mechanical science and technology*, 19(1):216–223, 2005.

[78] W. Souza. Basic cell biology of trypanosoma cruzi. *Current pharmaceutical design*, 8(4):269–285, 2002.

[79] W. d. Souza. Electron microscopy of trypanosomes: a historical view. *Memórias do Instituto Oswaldo Cruz*, 103(4):313–325, 2008.

[80] W. d. Souza. Structural organization of trypanosoma cruzi. *Memorias do Instituto Oswaldo Cruz*, 104:89–100, 2009.

[81] J. D. Stanaway and G. Roth. The burden of chagas disease: estimates and challenges. *Global Heart*, 10(3):139–144, 2015.

[82] J. Telleria and M. Tibayrenc. *American trypanosomiasis: Chagas disease one hundred years of research*. Elsevier, 2010.

[83] A. Trautmann. Extracellular atp in the immune system: more than just a "danger signal". *Sci signal*, 2(56):e6, 2009.

[84] K.-i. Tsubota. Elongation deformation of a red blood cell under shear flow as stretch testing. *Journal of the Mechanics and Physics of Solids*, 152:104345, 2021.

[85] K. Tyler and D. Engman. The life cycle of trypanosoma cruzi revisited. *International journal for parasitology*, 31(5):472–481, 2001.

[86] S. Uppaluri. Unicellular parasite motility: a quantitative perspective. 2011.

[87] G. Villalobos, F. Kun, and J. D. Muñoz. Effect of disorder on temporal fluctuations in drying-induced cracking. *Physical Review E*, 84(4):041114, 2011.

[88] F. Villalta, J. Scharfstein, A. W. Ashton, K. M. Tyler, F. Guan, S. Mukherjee, M. F. Lima, S. Alvarez, L. M. Weiss, H. Huang, et al. Perspectives on the trypanosoma cruzi–host cell receptor interactions. *Parasitology research*, 104(6):1251–1260, 2009.

[89] t. f. e. Wikipedia. The six main morphologies of trypanosomatids. `https://commons.wikimedia.org/wiki/File%3ATrypanosomatidMorphologies_PlainSVG.svg`, 2011. [Online; accessed October 26, 2015].

[90] B. J. Williams, S. V. Anand, J. Rajagopalan, and M. T. A. Saif. A self-propelled biohybrid swimmer at low reynolds number. *Nature communications*, 5, 2014.

[91] L. S. Wilson, A. M. Strosberg, and K. Barrio. Cost-effectiveness of chagas disease interventions in latin america and the caribbean: Markov models. *The American journal of tropical medicine and hygiene*, 73(5):901–910, 2005.

[92] D. M. Wootton and D. N. Ku. Fluid mechanics of vascular systems, diseases, and thrombosis. *Annual review of biomedical engineering*, 1(1):299–329, 1999.

[93] J. Zhang, P. C. Johnson, and A. S. Popel. Red blood cell aggregation and dissociation in shear flows simulated by lattice boltzmann method. *Journal of biomechanics*, 41(1):47–55, 2008.

7 APPENDIX

Seed 2	
Base Case	**Heart**
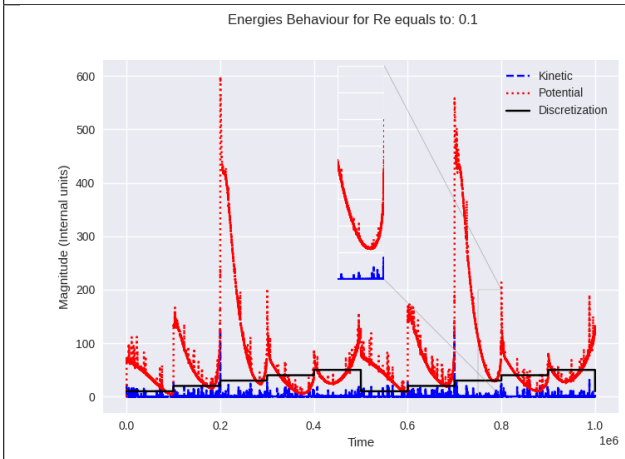	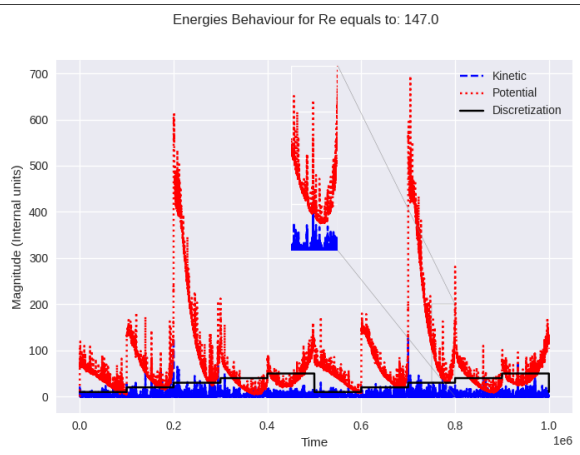
Oesophagus	**Colon**
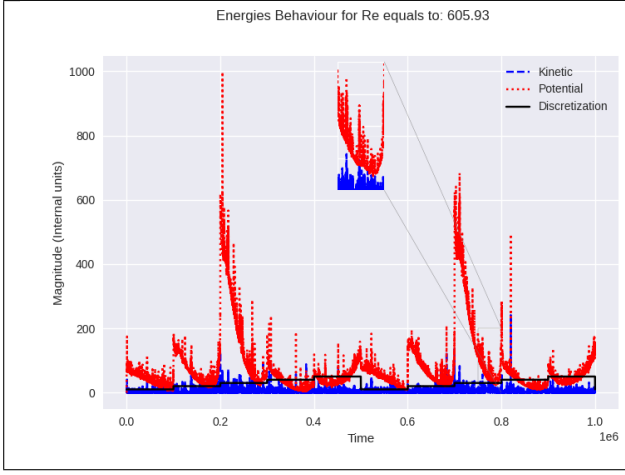	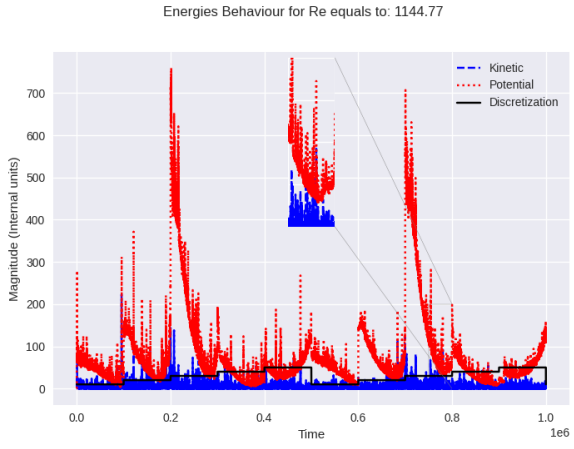

Table 16: Energies in parallel flow - Seed 2

Seed 3	
Base Case	**Heart**
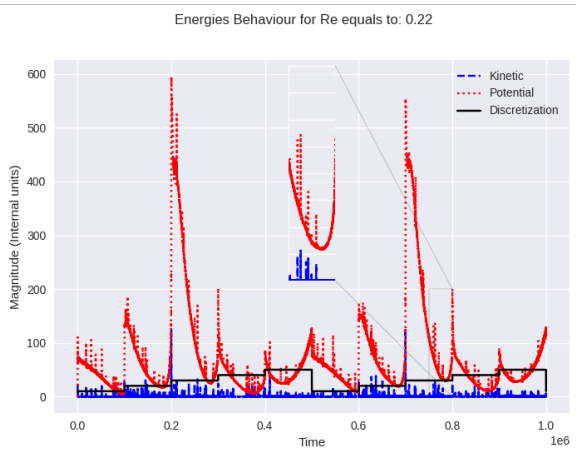	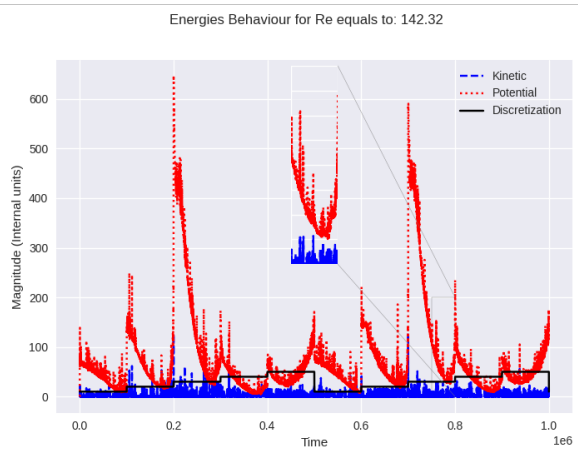
Oesophagus	**Colon**
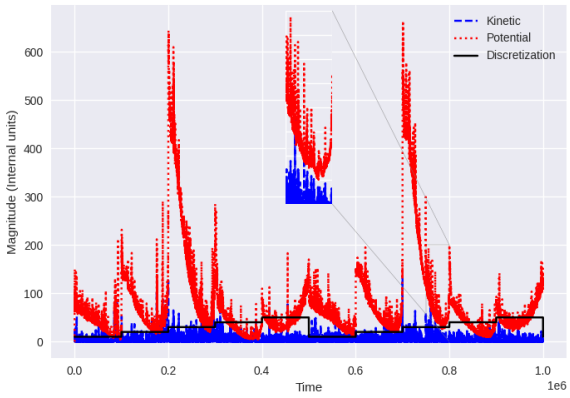	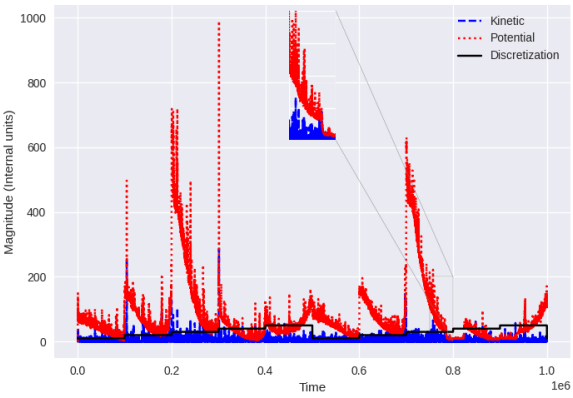

Table 17: Energies in parallel flow - Seed 3

Seed 2	
Base Case	**Heart**
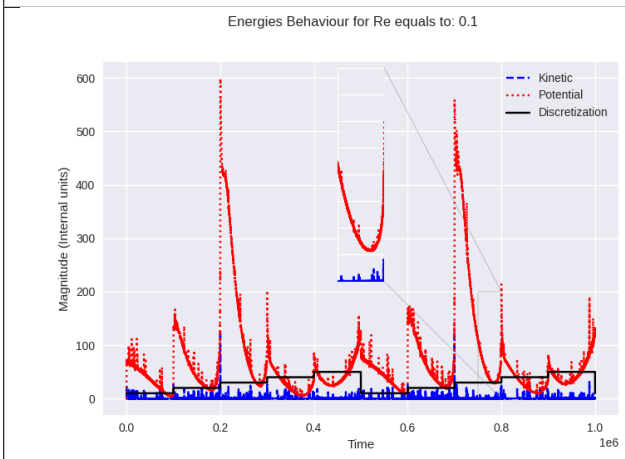	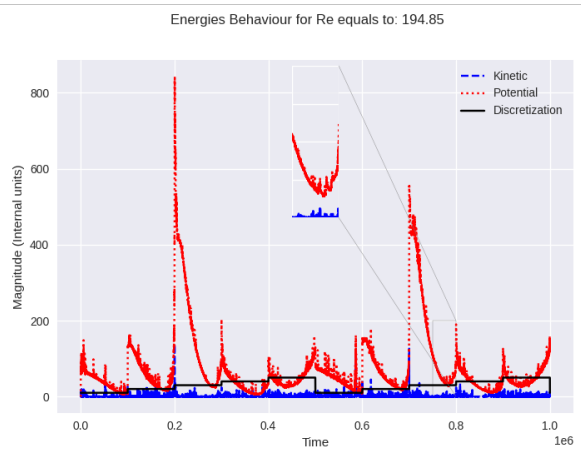
Oesophagus	**Colon**
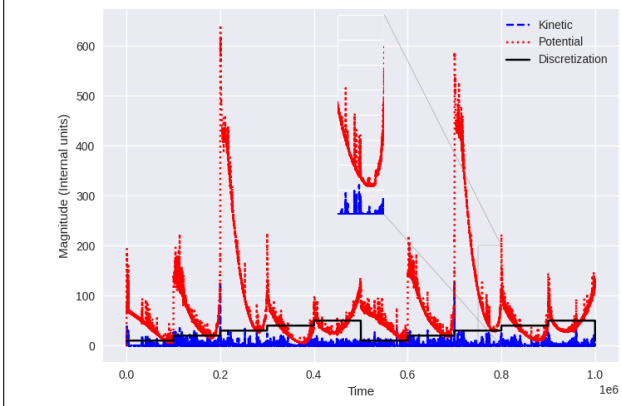	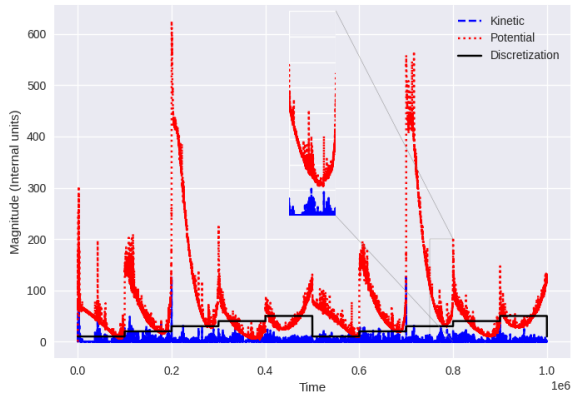

Table 18: Energies in perpendicular flow - Seed 2

Seed 3	
Base Case	**Heart**
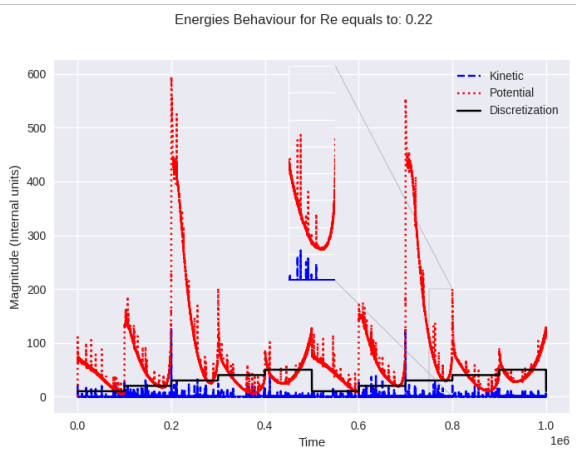	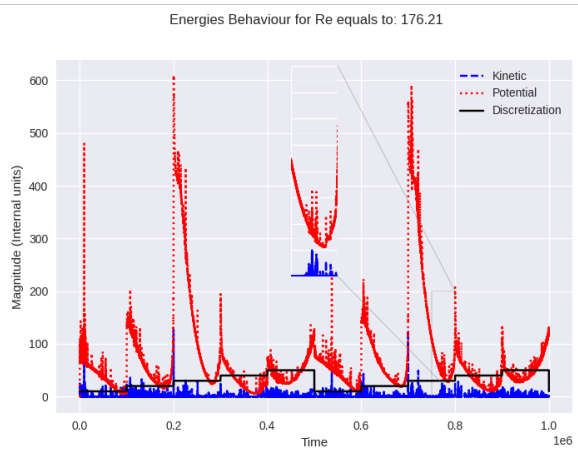
Oesophagus	**Colon**
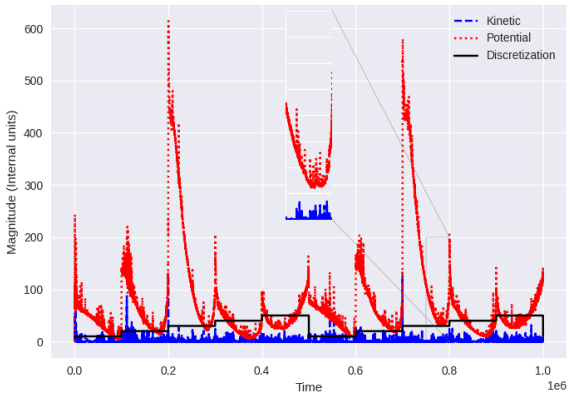	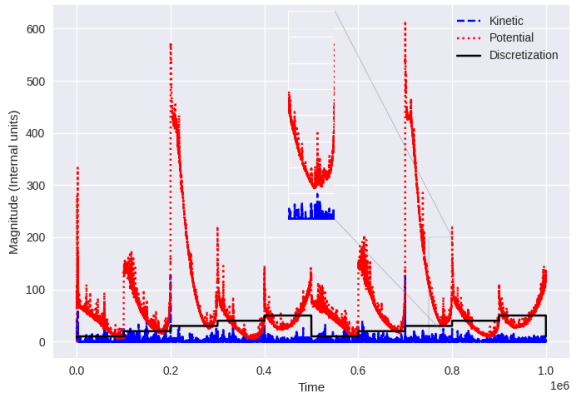

Table 19: Energies in perpendicular flow - Seed 3